framatome

Response to Request for Additional Information—BAW-10247, Supplement 3

BAW-10247,
Revision 0
Supplement 3Q1NP,
Revision 0

Topical Report

April 2026

FRAMATOME TRADEMARKS

ATRIUM and **Z4B** are trademarks or registered trademarks of Framatome or its affiliates, in the USA or other countries.

Nature of Changes

Item	Section(s) or Page(s)	Description and Justification
1	All	Initial Issue

Contents

List of Tables

List of Figures

Nomenclature

Acronym	Definition
3D	Three-dimensional
CI	Confidence Interval
Cr	Chromia
EEFGR	Extended Exposure Fission Gas Release
FA	Fuel Assembly
FGR	Fission Gas Release
FLFR	Full-length Fuel Rod
FR	Fuel Rod
FV	Free Volume
HBS	High Burnup Structure
HRX	Hardening Relaxation
LHGR	Linear Heat Generation Rate
NAF	Nuclear Absorber Fuel
NRC	Nuclear Regulatory Commission
PI	Prediction Interval
PLFR	Part-Length Fuel Rod
PPM	Parts-per-million
RAI	Request for Additional Information
RIP	Fuel Rod Internal Pressure
RPP	Radial Power Profile
RT	Room Temperature
RX/RXA	Recrystallized Annealed
SE	Safety Evaluation
SR/SRA	Stress-Relieved Annealed
TR	Topical Report
UGD	Gadolinia Doped UO2 fuel
UTL	Upper Tolerance Limit
Zry-4	Zircaloy-4

ABSTRACT

The United States Nuclear Regulatory Commission (NRC) provided a request for additional information (RAI) regarding the topical report BAW-10247P, Revision 0, Supplement 3, Revision 0. A total of six (6) questions were received from the NRC. This document provides the responses to those questions.

1.0 SUMMARY

The United States Nuclear Regulatory Commission (NRC) provided a request for additional information (RAI) regarding the topical report BAW-10247PA, Revision 0, Supplement 3, Revision 0 (Reference 1) in Reference 2. A total of six (6) questions were received from the NRC (Reference 2).

The following sections provide the responses to the NRC questions.

2.0 RAI 1

2.1 *RAI Text*

Framatome provided detailed Fission Gas Release (FGR) modeling information and comparison to high burnup data in Section 3.1.2, "G4-Fission Gas Release," of TR BAW-10247, Revision 0, Supplement 3. Rod internal pressure is proportional to FGR by the ideal gas law, which suggests that the rod internal pressure (RIP) model should continue to be acceptable for use at higher burnup. However, the RIP model is not qualified at the higher level of burnup requested within this supplement, and ample justification for the continued applicability of the RIP model into the burnup range requested is not provided within the TR.

The NRC staff requests that Framatome provide figures showing calculated vs measured RIP and RIP calculated vs measured vs burnup. Additionally, provide justification via analysis and/or comparison to data at higher burnup levels showing that the RIP model is applicable for use at the higher burnup requested without additional validation.

2.2 *RAI Response*

BACKGROUND

Information regarding fuel Rod Internal Pressure (RIP) and Free Volume (FV) measured after irradiation is available for the Extended Exposure Fission Gas Release (EEFGR) dataset for which only FGR benchmarking was presented in Supplement 3 to the topical report (Reference 1). Benchmarking RIP and FV for the nominal exposure range (up to **[ ]** MWd/kgU FLFR) was presented in the initial topical report (Reference 4) and was accepted by the NRC in their review of that topical report. Below, the benchmarking of RIP and FV to an extended burnup range of up to **[ ]** MWd/kgU is described and discussed.

The procedure of fuel rod puncturing in the hot-cell after irradiation provides RIP and FV at RT (hot-cell temperature) in addition to the FGR (absolute and relative units). Usually, when puncturing the fuel rod in the hot cell, a “double expansion” procedure, provides both the RIP and FV of the examined fuel rod.

The composition of the collected gas from the fuel rod is measured by a Mass Spectrometer on a sample taken from the collected gas to determine FGR. FGR which occurred during operation results in additional gas amount that is added to the initial, as manufactured, fill gas, and the % FGR is calculated as the ratio of the measured amount of fission gas to the calculated total fission gas produced (stable Xe and Kr isotopes), based on measured or calculated burnup.

The ideal gas law links together the amount of FGR, ν_{fgr}, expressed in moles, the RIP and the FV, as shown below by Eq. 2-1:

$$RIP \cdot FV = \left(\nu_{fgr} + \nu_{fill}\right) \cdot R \cdot T \qquad \text{Eq. 2-1}$$

Therefore, RIP is proportional to FGR ($the\ \nu_{fgr}$ term) and inversely proportional to FV, so that good agreement for RIP implies good agreement for both FGR and FV, and vice-versa. The relation of Eq. 2-1 will be used later to discuss the benchmarking results that are presented below.

BENCHMARKING RESULTS

The comparison between measured and calculated RIP for the EEFGR dataset is presented in Figure 2-1 and the best-estimate results with uncertainty differences are similar to the benchmarking for nominal exposure as shown in the original topical report (Reference 4, Figure 4.13).

Figure 2-1
Measured vs calculated RIP values for the EEFGR dataset

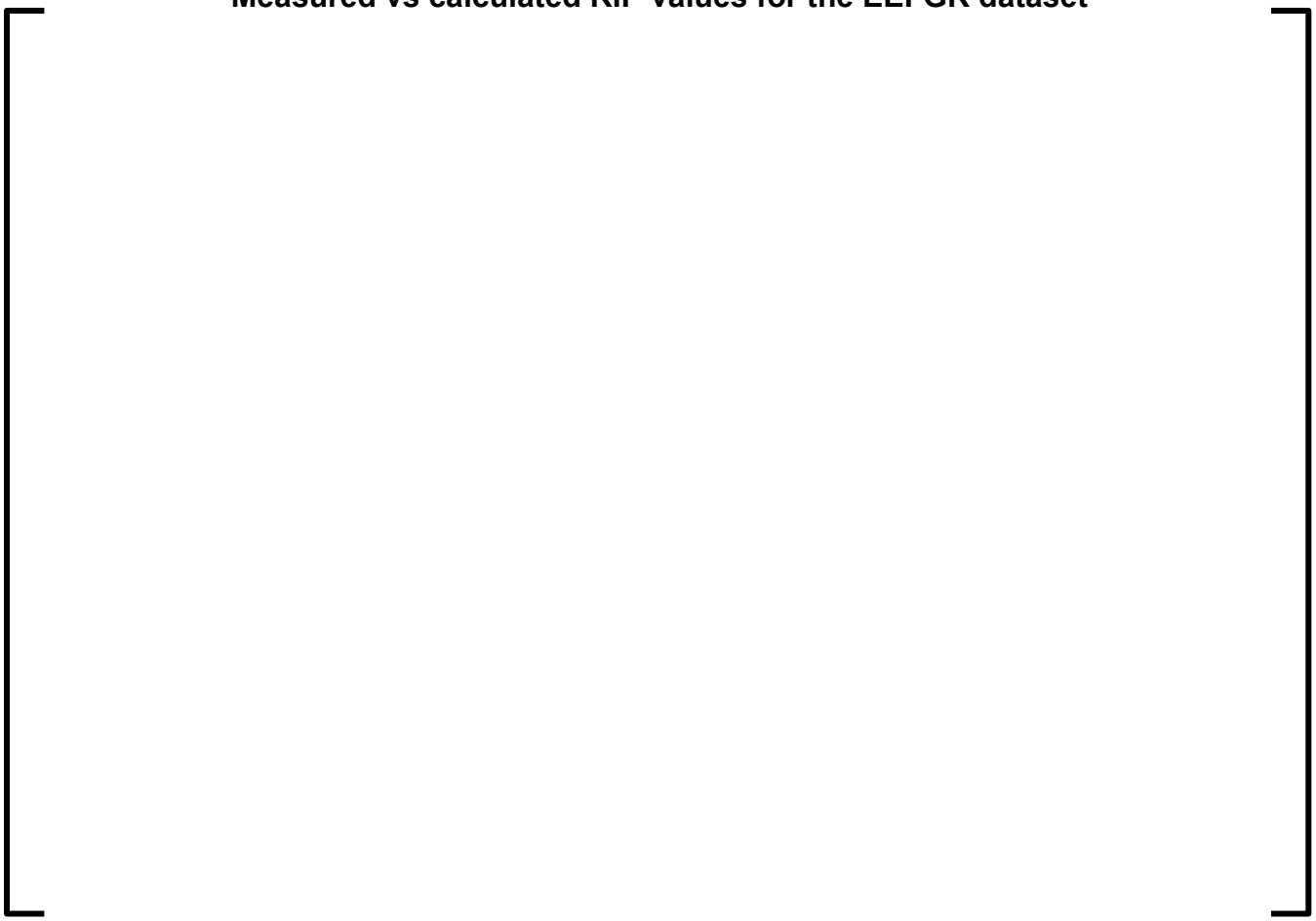

Figure 2-2 shows the evolution with exposure of both calculated and measured RIP for the EEFGR dataset. Consistent agreement along the whole burnup range is noted between calculations and measurements. One datapoint with larger difference between calculation and measurement is noted at about [ ] which appear as an outlier being surrounded by good agreement data at lower and higher burnups. The reasons for this outlier and its resolution are discussed later.

Figure 2-2
Full-Length Fuel Rod-averaged Exposure vs calculated and measured RIP values for the EEFGR dataset

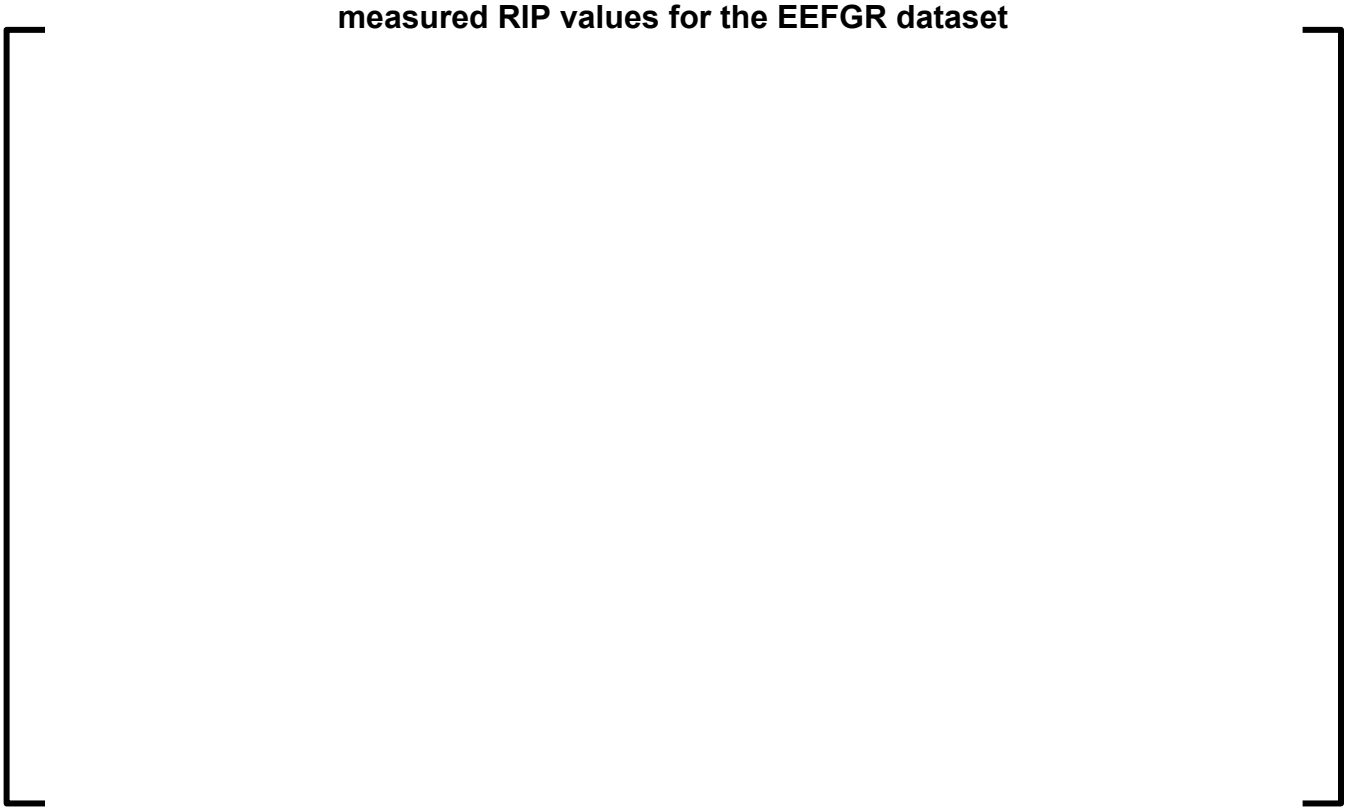

The FGR measurements on fuel rods from assembly [ ] were presented in the Supplement 3 topical report (Reference 1) because the measured fuel rods were discharged at increasing exposures so that a good representation of FGR evolution with exposure was achieved up to the extended exposure range. The benchmarking of RIP shown in the two previous figures is illustrated in Figure 2-3 and Figure 2-4 below for the EEFGR dataset. Good agreement is noted in these two figures, which shows that the evolution of RIP with exposure is captured well.

Figure 2-3
Measured vs calculated RIP values for the 1601 dataset

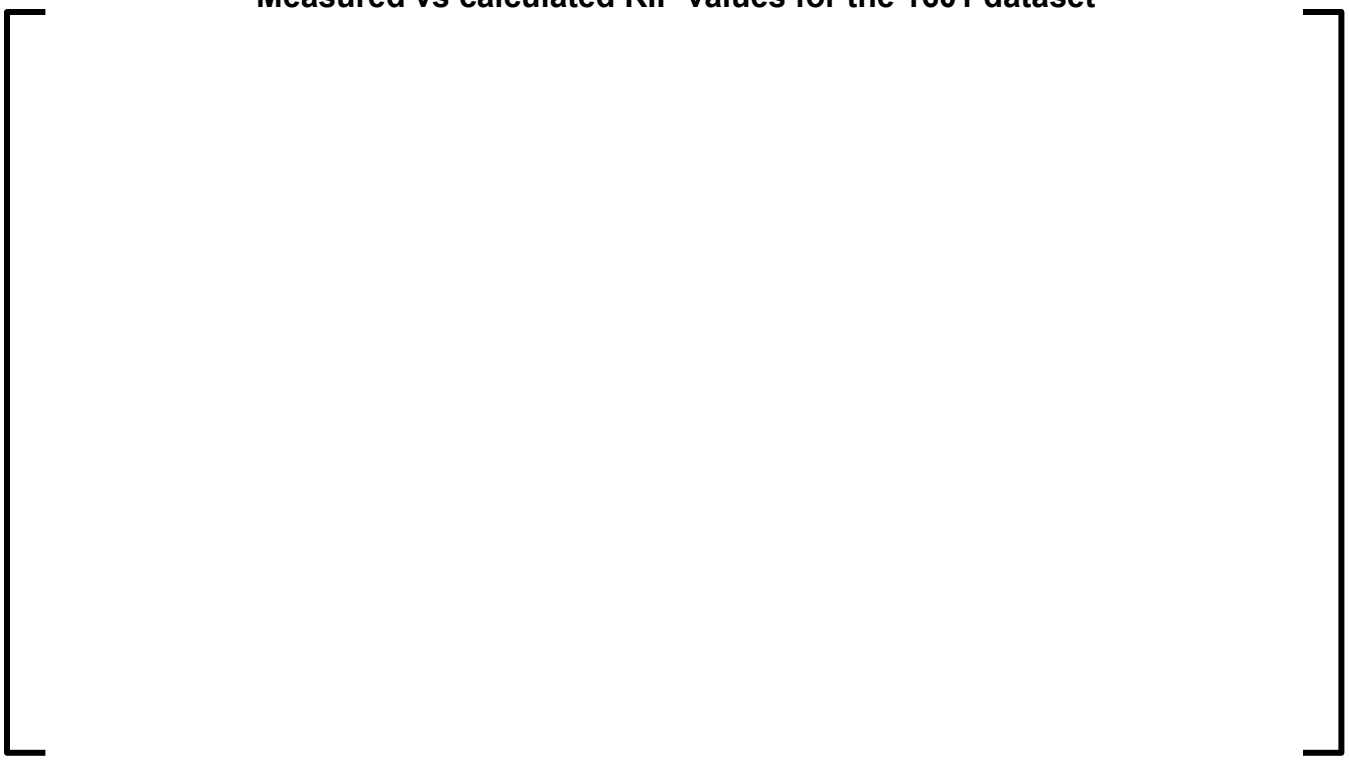

Figure 2-4
RIP versus Full-length Fuel Rod Exposure for the 1601 dataset

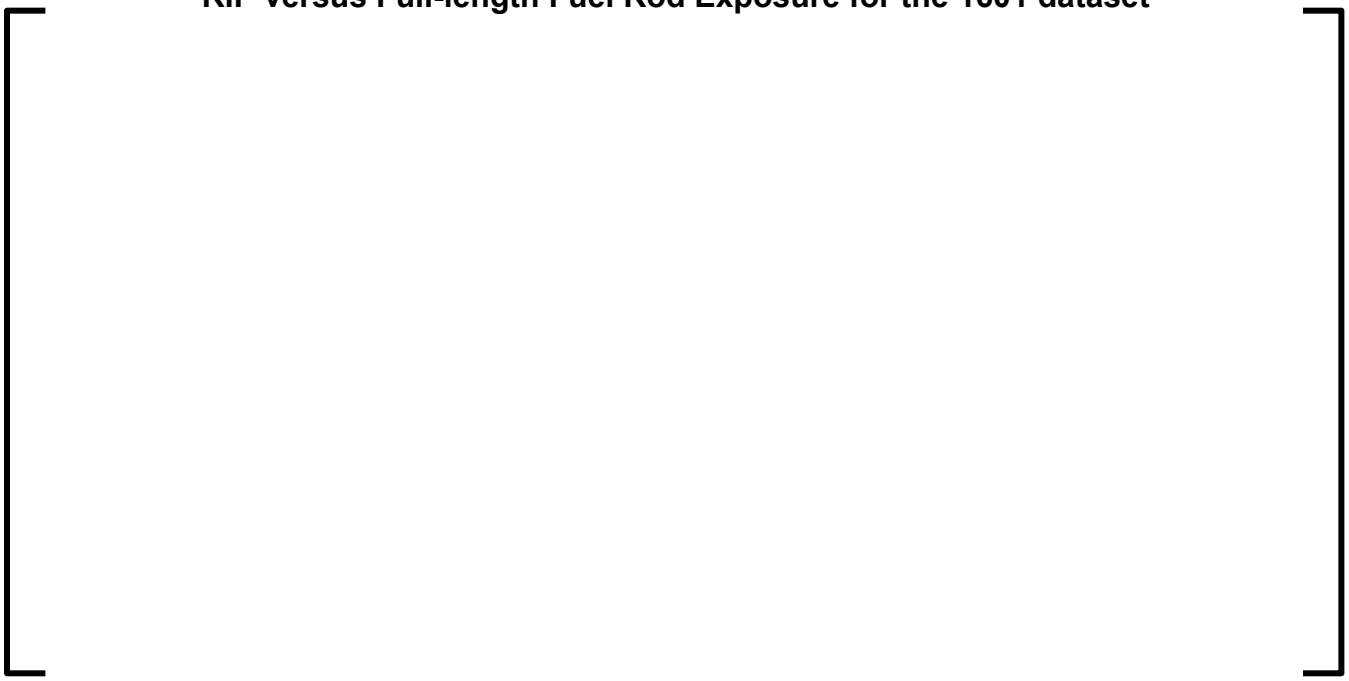

Because FV is the other parameter, besides FGR, involved in determining RIP, the benchmarking of FV for the EEFGR and [ ] datasets is presented in Figure 2-5 and Figure 2-6, and Figure 2-7 and Figure 2-8, respectively. Similarly good best-estimate results with a typical uncertainty range (similar to that of nominal exposure results, as shown in the original topical report (Reference 4, Figure 4.28)) is noted; this supports the consistent modeling of RODEX4 in that all separate processes contributing to RIP are adequately modeled. The discrepancy that is observed at about [ ] in Figure 2-6 is related to the outlier noted above and will be discussed later.

Figure 2-5
Measured FV vs calculated FV for the EEFGR dataset

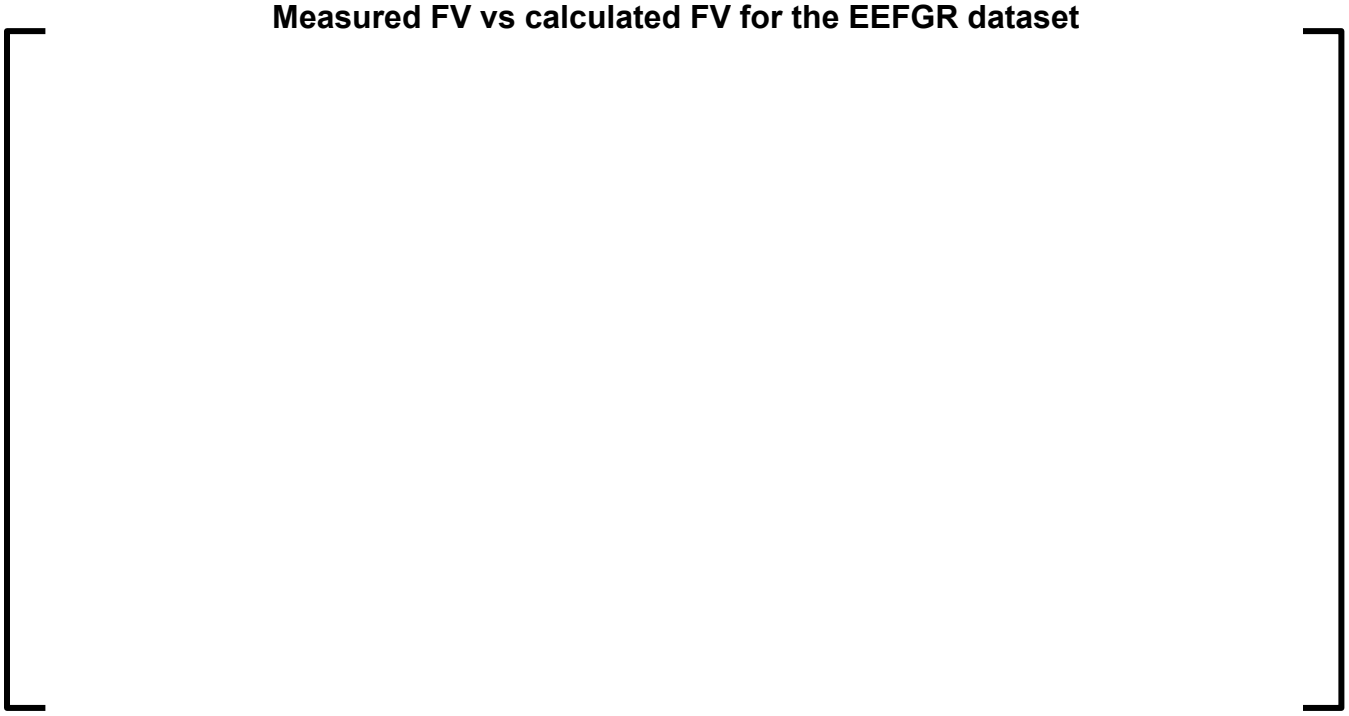

Figure 2-6
FLRA burnup vs calculated and measured FV for the EEFGR dataset

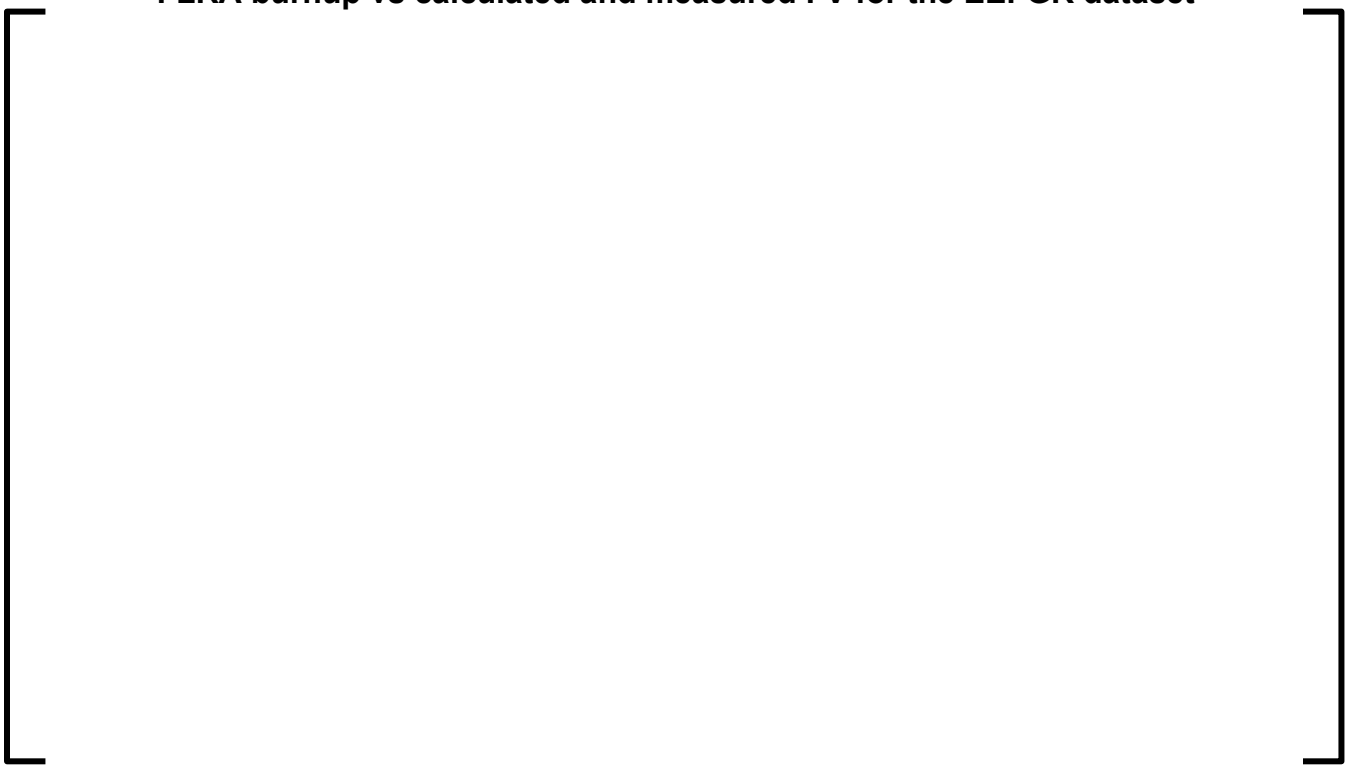

Figure 2-7
Measured FV vs calculated FV for the 1601 dataset

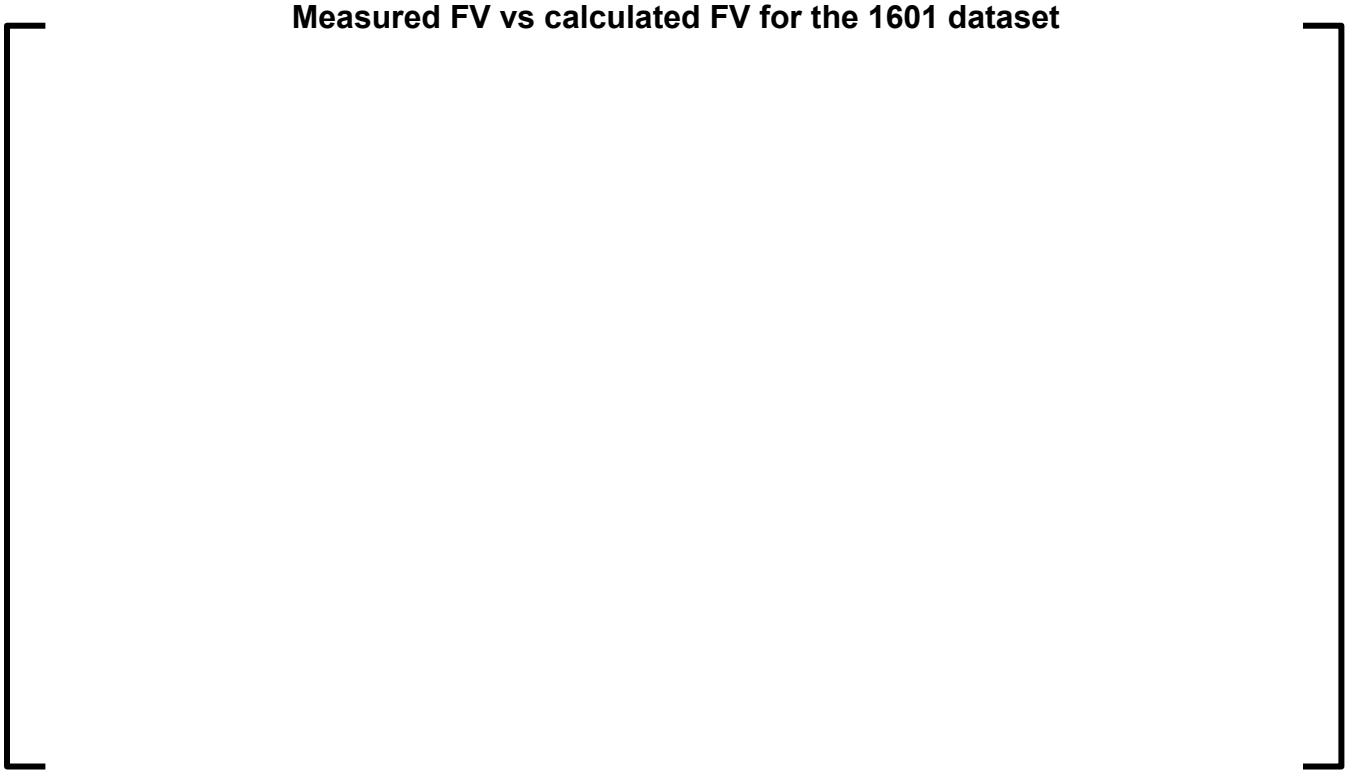

Figure 2-8
Full-length Fuel Rod averaged exposure vs calculated and measured FV for the 1601 dataset

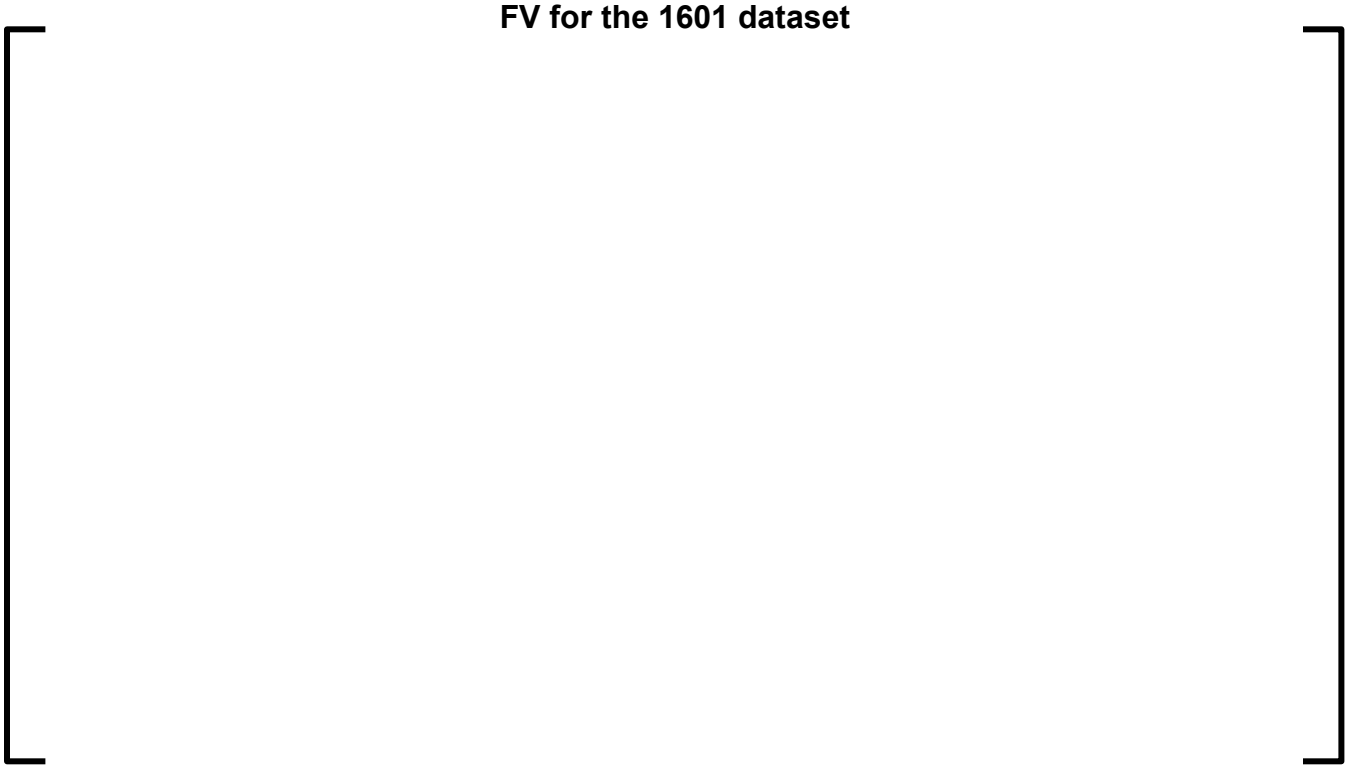

DISCUSSION

Good agreement between calculated and measured values is noted for both RIP and FV, which further supports the good agreement noticed for FGR for the extended burnup range.

There is one outlier at [ ] with measured RIP well above the trend of the other data (best seen in Figure 2-2), and for which an underprediction occurred. The FV for this outlier fuel rod is at the lower bound of the data range and significantly below the other high exposure data points (see Figure 2-6) and was overpredicted by RODEX4, while the predicted FGR agrees very well with the measured (Reference 1, Figure 3.3).

Based on Eq. 2-1, it can be inferred that cause of underpredicting the RIP for that outlier is that the FV was overestimated by RODEX4; this, indeed causes RIP to be underestimated, even if FGR is predicted within a negligible 0.3% difference from measurement.

This was confirmed by the details of the RODEX4 simulation of the [ ] outlier case, which indicated that the cladding axial elongation (also measured after irradiation) was greatly overestimated by RODEX4. This caused an increase in the plenum volume, which is the main contributor to FV. It was noted that the elongation of the [ ] fuel rod was considerably lower than the other fuel rods with nominal Zr alloy cladding, which shows that the RODEX4 model that was calibrated for standard Zr alloys is not capturing exactly cladding irradiation growth of the experimental cladding of the [ ] outlier.

Therefore, the reason for the RIP discrepancy for the [ ] fuel rod, is that the elongation of the cladding for that outlier fuel rod was an experimental Zr alloy variant and its creep and irradiation growth properties were different from the reference cladding materials modeled by the code. That Zr alloy variant was not implemented in production and full analysis of its mechanical and irradiation growth properties were not finalized.

The FGR is not affected by the discrepancy in the calculation of the plenum volume and therefore, this datapoint is relevant for the verification of FGR for the expected exposure range. The capability of RODEX4 to predict FGR for the extended exposure range is supported by Figure 2-9 below, which shows that the best-estimate and the same uncertainty range as for the nominal exposure range.

Figure 2-9
Measured vs calculated FGR for the initial and EEFGR datasets

3.0 RAI 2

3.1 *RAI Text*

Framatome provided within Figure 3-6, "Exposure Range for Cr-doped Fission Gas Release Dataset," of TR BAW-10247, Revision 0, Supplement 3, a dataset of FGR for Chromia (Cr) doped fuel at higher burnup which indicates that higher burnup datapoints were used to calibrate RODEX4. However, this dataset does not demonstrate RODEX4's predictive capabilities of FGR for Cr doped fuel at the burnup range requested, as only the measured quantity of FGR is shown. Framatome provided multiple figures in its response to RAI 8b within ANP-10340Q1P, Revision 0 (ADAMS Package Accession No. ML18171A107) demonstrating RODEX4's ability to predict Cr doped fuel FGR at a comparable level to non-doped. Similarly, the figures within the response did not adequately demonstrate RODEX4's capability to accurately and reliably predict Cr doped fuel FGR at the higher burnup range requested for approval within Supplement 3.

Therefore, the NRC staff requests that Framatome provide a figure that shows RODEX4's performance against FGR data for Cr doped fuel. For example, generating a figure similar to Figure 3-3, "High Exposure Dataset, Calculated and Measured Fission Gas Release Values," plotting the Cr doped dataset provided within Figure 3-6 alongside RODEX4's predictions.

3.2 *RAI Response*

The FGR benchmarking results for the Cr-doped dataset, together with the measured values, have been re-plotted as function of rod average burnup in Figure 3-1 below.

Figure 3-1
Rod average (FLRA) burnup vs calculated and measured FGR for Cr-doped data

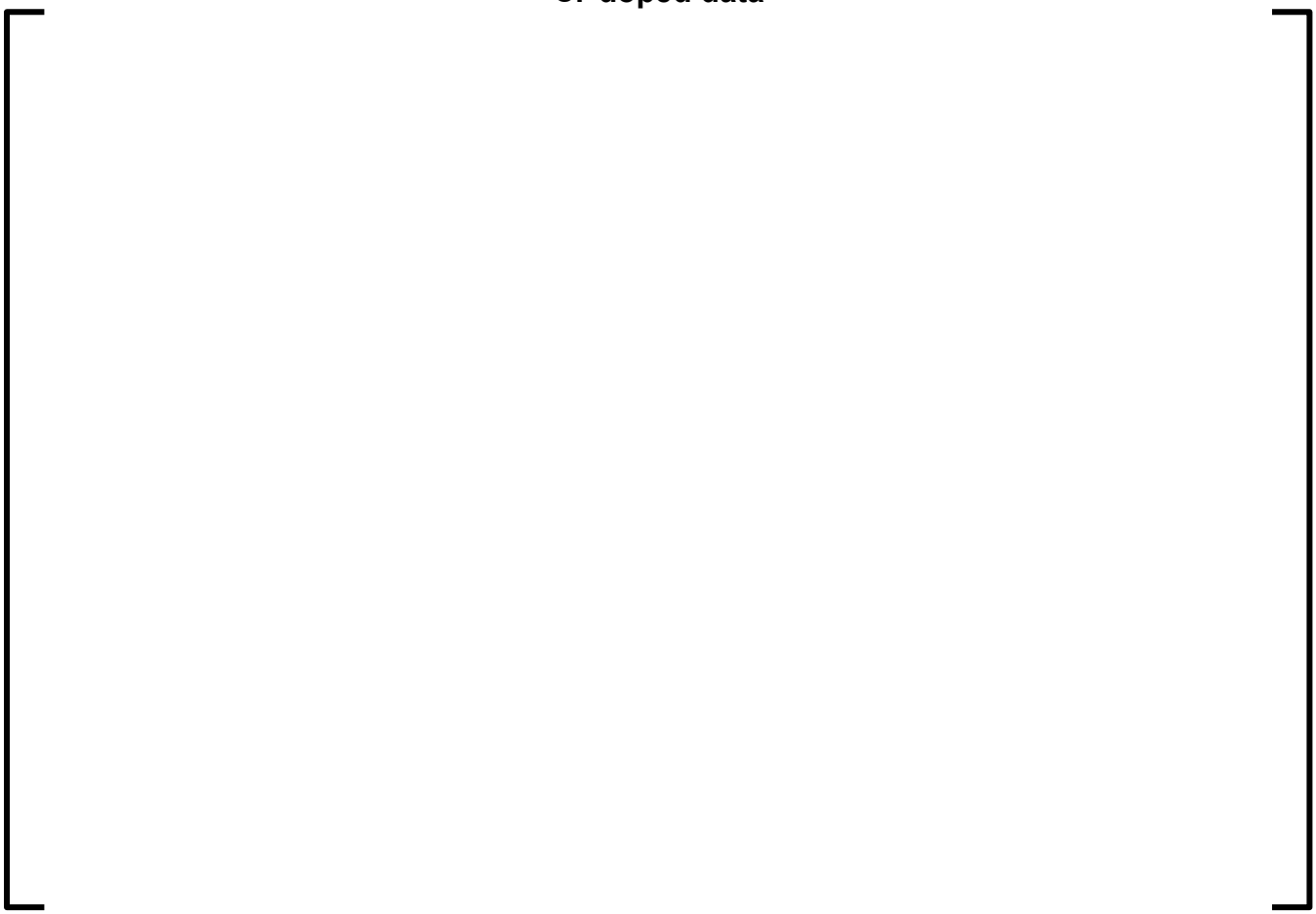

It may be noted that the calculated results bound the measured values for high FGR. To demonstrate best-estimate and no bias with exposure, the delta FGR, i.e., the difference between calculated and measured FGR values, is plotted as a function of exposure in Figure 3-2. The same spread of the delta FGR for the whole burnup range indicates that RODEX4 FGR model has no bias with exposure.

The overall best-estimate prediction of the Cr-doped database was demonstrated in the topical report for including Chromia in fuel pellets (Reference 5); in addition, the continued applicability of the FGR model uncertainty for Cr-doped fuel was demonstrated in response to an additional request for clarification and illustrated in Figure 3.4-1 of the Safety Evaluation (SE) for that topical report (Reference 5).

Figure 3-2
Delta (difference between calculated and measured) FGR values as function of FLRA burnup for the Cr-doped dataset

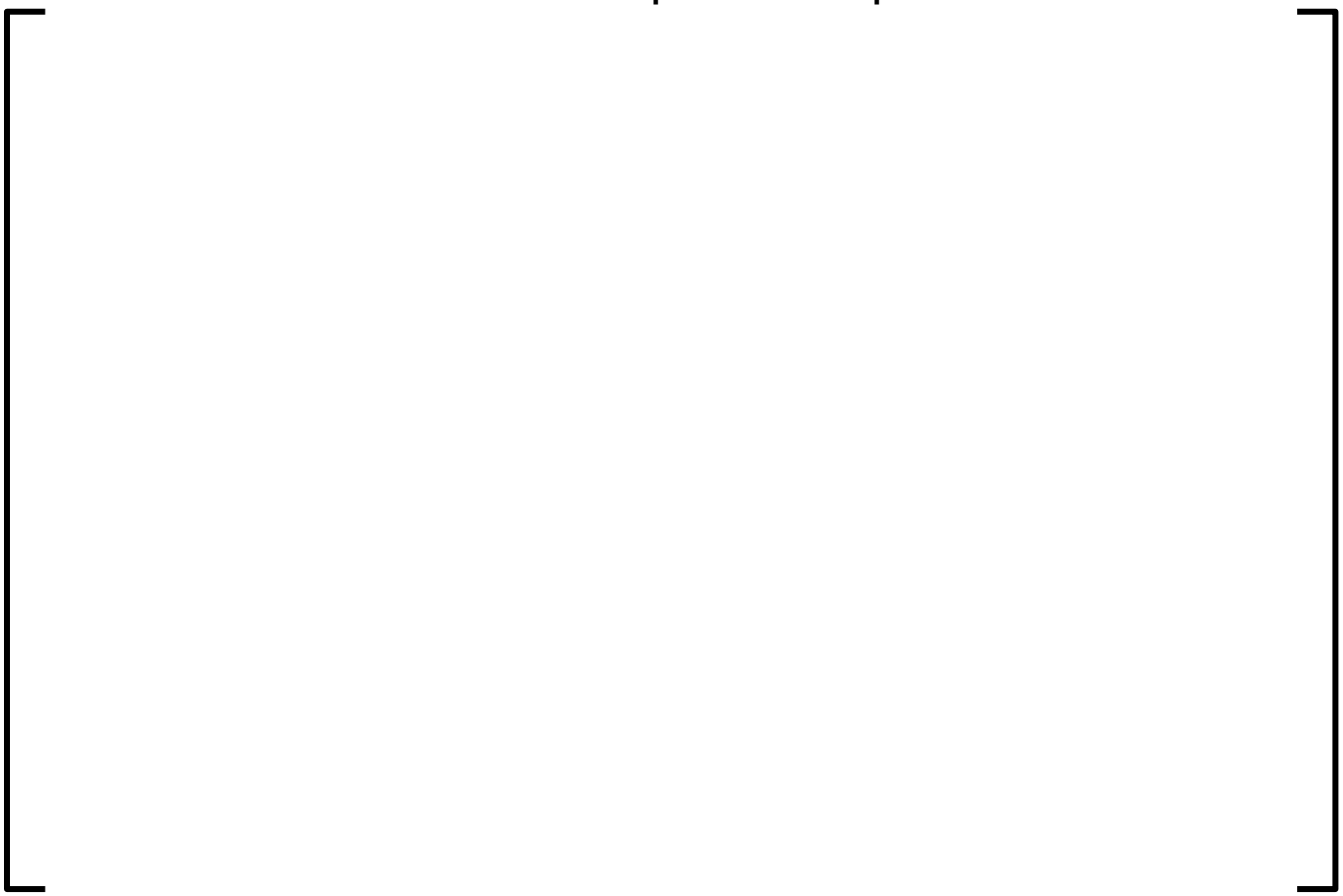

4.0 RAI 3

4.1 *RAI Text*

Section 5.3, "Extension of NAF RPP Correlations for Higher Enrichments," of TR BAW-10247, Revision 0, Supplement 3, indicates the existing radial power profile (RPP) tables in RODEX4 have an upper bound enrichment of 5 weight percent (wt%) uranium (U)-235 for both gadolinia and non-gadolinia fuel. The RPP entries in these tables were derived for specific combinations of relevant parameters by using **[ ]** to process RPP values that were generated via **[ ]** for a wide range of parameters. Section 5.3 of the TR also indicates that the updated version of **[ ]**, was used to extend the enrichment range of non-gadolinia fuel to 10 wt% U-235 and that the extension of gadolinia tables above 5 wt% U-235 followed the same procedure used in GALILEO. Based on the TR submittal, it is not clear to the NRC staff how RODEX4 processes the transition from one range of U-235 enrichment generated from one code to another range generated by another code. Additionally, in a regulatory audit conducted from September 9, 2025, to September 11, 2025 (ADAMS Package Accession No. ML25212A128), Framatome indicated RPPs for higher enrichments were developed using **[ ]**.

The NRC staff requests that Framatome provide discussions detailing the manner in which the RPPs were generated using **[ ]** and the relationship between these RPPs and the RPP tables used in the version of RODEX4 for which NRC-approval is being sought (e.g., are the **[ ]** RPPs processed by **[ ]** to generate the updated RODEX4 RPP tables)? Additionally, please clearly identify which enrichment ranges of RPPs are attributed to which code and discuss how RODEX4 processes the transition from one range to another. Lastly, please provide an example RPP plot of power density versus pellet radius from APOLLO2-A.

4.2 *RAI Response*

EXTENSION OF RPP TABLES TO HIGHER EXPOSURE

The original RODEX4 fuel code included radial power peaking (RPP) tables derived with [ ] from RPP values generated with [ ] for a range of geometric, operational, fuel composition and enrichment ranges. While the [ ] code was used to generate the power profile values for a calculation matrix covering the range of the relevant parameters: enrichment, Gd content, pellet outer radius, void fraction and rod average burnup, a response surface function type correlating these [ ]-calculated values was developed and implemented in a computer code, named [ ] whose outcome consists of a set of tables for the variation with burnup of the coefficients of the response surface function. The original version of [ ] that was used to prepare the RODEX4 RPP tables covered an enrichment range of up to 5% U-235 for commercial PWR and BWR fuel.

After the submittal of RODEX4 topical an updated versions of [ ] namely [ ] was used to extend the enrichment range to 10% U-235, except for the Gadolinia fuel, in which case the maximum U-235 enrichment remained at 5%. The burnup extended tables produced with [ ] are consistent with the original [ ] tables because the same methodology was used in both cases. Therefore, the burnup extended tables were implemented in RODEX4 for standard UO_2 fuel with U-235 enrichment above 5%.

A different method for the extension of U-235 enrichment range for Gadolinia fuel was necessary for the application of RODEX4 to higher than 5% U-235 enrichment. Because of numerical difficulties in using [ ] for this task, [ ] was used instead. Consequently, the RPP modeling in the new version of RODEX4 includes the initial [ ] RPP tables, the extended [ ] tables and the [ ] tables for Gadolinia fuel. The latter are used for U-235 enrichment greater than 6 %, with the 5% to 6% U-235 interval being used to transition between the initial [ ] tables and [ ] tables.

The structure of the decisional branches for the RPP calculations is illustrated in Figure 4-1 below. Based on the input U-235 enrichment and Gd content, the three branches in Figure 4-1 are selected. The original [ ] tables are used for the leftmost branch, while the middle branch represents the extended [ ] tables. The right-most branch is the newly developed [ ] -based RPP tables for Gd content higher than 5%. In between the middle and the right branches, the interpolation box represents the transition from the original [ ] and the new [ ] RPP tables for Gd content between 5% and 6%.

Figure 4-1
Block diagram of RPP modules for extended enrichment range

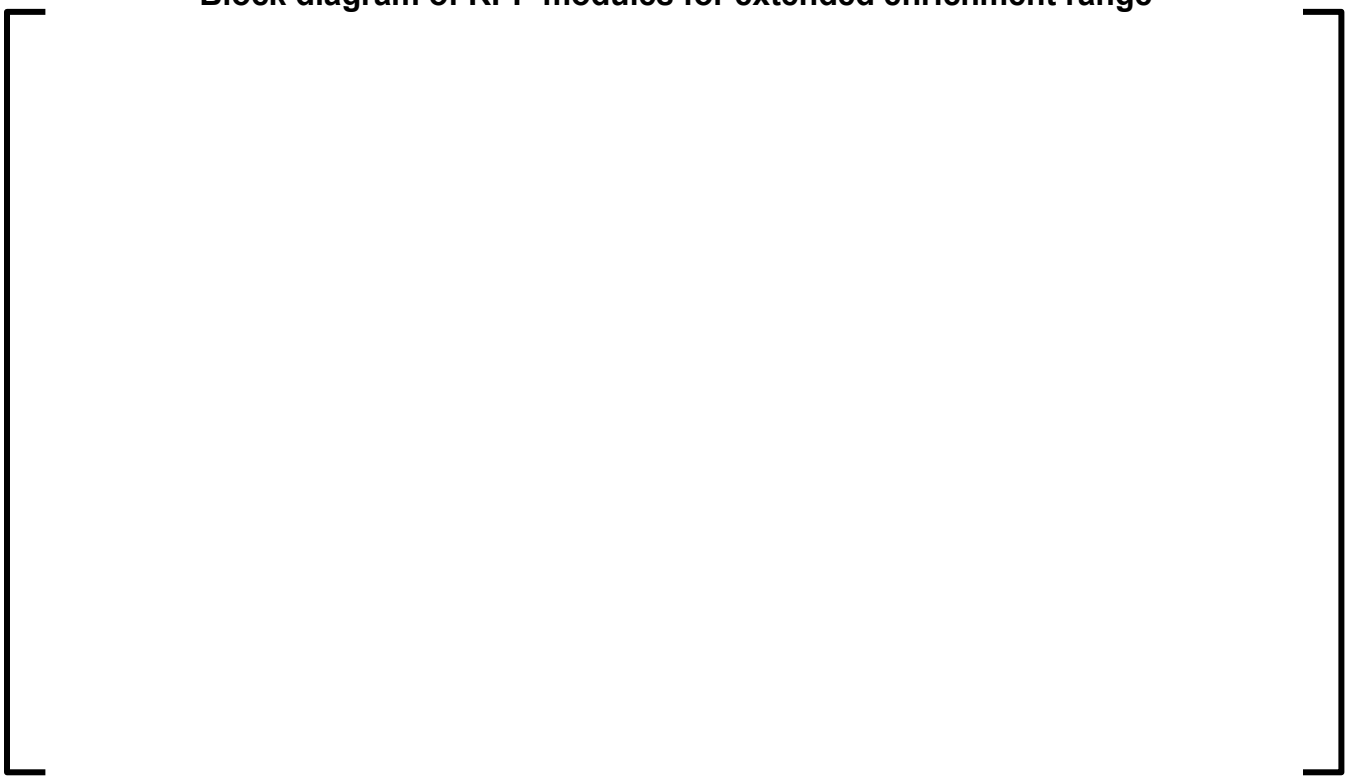

NEW INTERPOLATING TABLES FOR [ ] RPP CALCULATIONS

[ ] has the capability of refining the radial discretization and a refined exposure mesh is possible. This resulted in an enriched RPP dataset produced with **[ ]** which allowed a more direct approach for the RPP tables than the **[ ]** post-processing procedure. Instead of fitting a response function like **[ ]** was developed to interpolate the **[ ]** RPP values and convert to a different radial mesh as used in RODEX4.

Also, the RPP values are normalized to the pellet average linear heat generation rate and are paired with the fractional pellet radius at mid-ring locations. However, for the conversion of the [ ] RPP to a different radial mesh, the nodal RPP values are also needed.

In [ ] the pellet is divided into "N" contiguous rings. The corresponding nodal radial mesh, (rn(j), j=1, N+1), which identifies the left and right ends of each ring, is constructed by the following algorithm, based on the definition of the mid-ring radii, (rr(i),i=1,N) as the arithmetic average of the end radii of that ring, namely rn(i) and rn(i+1):

Leftmost radial node:

$$\boldsymbol{rn(1) = 0}$$ (no hollow pellet in [ ] analyses) Eq. 4-1

Recursive relation:

$$\boldsymbol{rn(i+1) = 2 \cdot rr(i) - rn(i)}$$ for i = 1 to N Eq. 4-2

This procedure is illustrated in Figure 4-2, with the radial nodes on the x-axis. The next step is to derive the nodal RPPs for the given [ ] radial mesh defined above.

The basis for the calculation of the nodal RPPs is the premise of [ ] within each ring, which is the assumption made in the RODEX4 temperature solver where the RPPs are utilized. Because of the cylindrical geometry, the average value of a given ring is not equal to the arithmetic average of the ring end values (as it is for plane geometry) and the parameters of the [ ] for a ring defined by inner, r_j, and outer, r_{j+1}, boundaries, are calculated from the definition, as follows (index j for y and y_{av} are omitted in Eq. 4-3 and Eq. 4-4 below):

[ ] Eq. 4-3

Assuming [ ] within the ring:

[ ] Eq. 4-4

Introducing Eq. 4-4 into Eq. 4-3, the average y value for the "j" ring [r_j , rj_{+1}] is calculated as:

[ ] Eq. 4-5

It is remarked that for a fine mesh and away from the center of the pellet, in which case the end radii r_j and r_{j+1} are not very different, the [ ] parameter β of Eq. 4-5 is very close to 0.5, as for a plane geometry.

By using Eq. 4-5, the nodal RPPs can be estimated recursively by first implementing the condition of extremum at the pellet center, which means a zero first derivative. This condition is translated for the radial discretization utilized in both the neutronic lattice and fuel codes, [

]

[ ] Eq. 4-6

Then applying Eq. 4-5 recursively, the nodal value yn(i+1) at the right end of ring i, is calculated as:

[ ] Eq.4-7

The result of this algorithm to construct the set of nodal values from given ring average values are illustrated in Figure 4-2, with a detailed view in Figure 4-3.

Figure 4-2
Nodal RPP values determined from ring average values

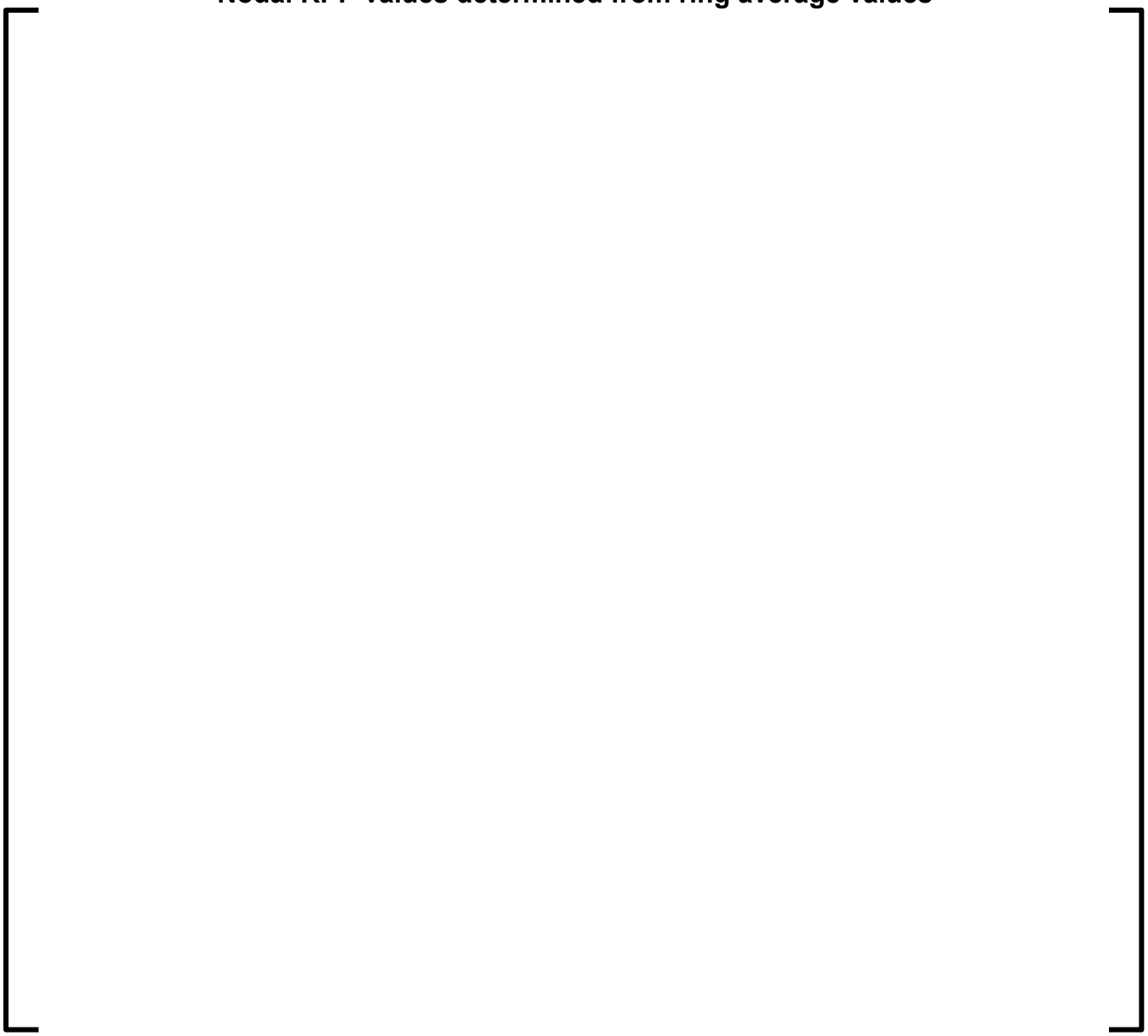

Figure 4-3
Detail view of nodal values determination

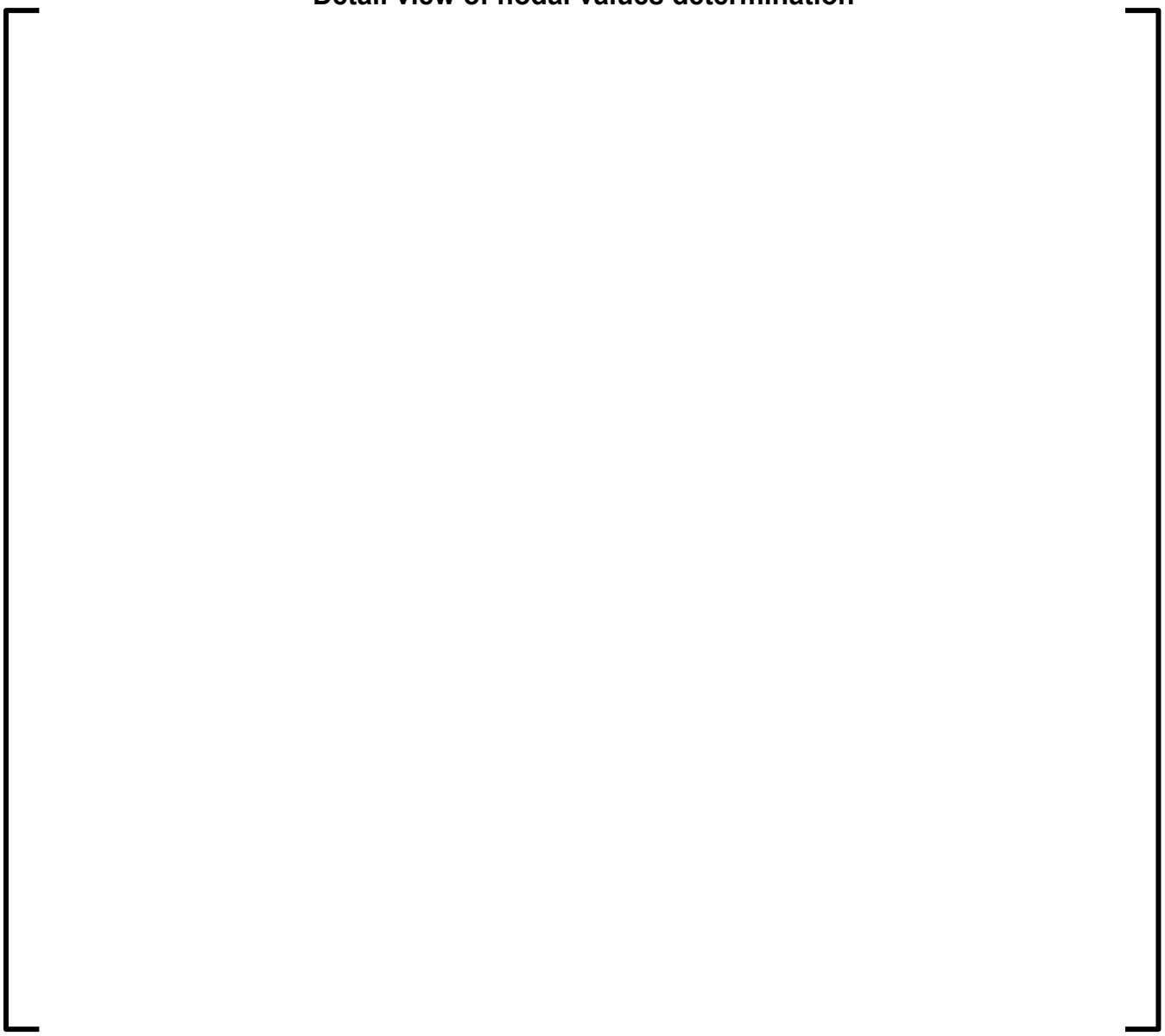

Once the [ ] ring average and nodal RPPs are established as described above, the same can be inferred for the RODEX4 radial discretization mesh. First, the conversion to RODEX4 ring average RPPs, (yrd(i),i=1,NRD-1) is achieved as follows.

The first step is to identify the [ ] ring within each RODEX4 nodal boundary is contained. Then, the position of the RODEX4 rings relative to the [ ] radial mesh is determined, based on the location of the two boundaries of each ring. Two situations can occur:

a) the RODEX4 ring is fully contained in a certain [ ] ring, or

b) the RODEX4 ring spans one or more [ ] rings.

In case b), the RODEX4 ring consists of full [ ] rings or sub-intervals of [ ] rings, at the left or right boundaries of the RODEX4 ring.

The procedure for calculating the average RPP value for sub-intervals, which occurs for either case a) or case b), is based on the same [ ] that was mentioned above (Eq. 4-4). Using the inferred [ ] nodal RPPs and the respective radial coordinates of the sub-intervals, the end values of those sub-intervals are calculated, according to Eq. 4-4, which then can be used to calculate the average over the respective sub-interval, according to Eq. 4-5.

The final step is to calculate the RODEX4 nodal RPPs by using Eq. 4-6 and Eq.4-7.

DESCRIPTION OF THE [ ] RPP CALCULATIONS

The assumptions used to perform RPP calculations with the [ ] methodology, namely the estimate of an equivalent homogenous lattice pitch, led to difficulties with higher enrichment and gadolinia in the fuel. These difficulties can be addressed by using a higher order method with explicit heterogeneous lattice geometry modeling capability to generate the RPP instead. Using [ ] for this purpose is adequate because [

]

The accuracy of [ ] for calculating RPP on a fuel pellet mesh consistent with this analysis has been verified by comparison to SERPENT 2.1.31, a high-resolution Monte Carlo neutronics code. It was shown to be accurate to within a relative difference of [ ] for the relevant figure of merit described below. Accuracy of the code was further demonstrated in [

]

The radial power profiles were generated using the following high-level procedure.

1. Set up and run [ ] for representative lattice designs using higher radial power profile fidelity in the gadolinium fueled locations. These calculations were done with variation in the enrichment, coolant void, and gadolinium concentration within each gadolinia rod location. This was done to cover the desired range of each variable forming a tensor product of cases.

2. For each lattice design and enrichment/gad/void case, aggregate the radial power profiles [

]

3. The resulting RPP was normalized such that average LHGR of the ring is preserved when scaled to the pellet LHGR.

The [ ] calculations were set up [

] The refinements matched those used in the code verification activities described above.

The three pellet radii RPPs are generated with the corresponding representative fuel design.

- ATRIUM-9, Rpel=0.4746 cm
- ATRIUM 10XM, Rpel= [ ] cm
- ATRIUM 11, Rpel= [ ] cm

To ensure that the environment of the gadolinia fuel rods is adequately represented for each fuel type, one lattice for each of the mechanical zones (i.e., lattice zones for each of the different number of PLFRs) were used for each of the representative fuel designs. For instance, the three geometries analyzed for ATRIUM 11 fuel are given in Figure 4-4 where the gadolinia rod locations are highlighted in orange, and the water locations are highlighted in blue.

Figure 4-4
ATRIUM 11 Gadolinia RPP Locations

[ ]

For each enrichment, gadolinia concentration, moderator void, and burnup point there are radial power profiles corresponding to each of the gad locations from all geometries. For ATRIUM 11, this is equal to 23 unique radial power profiles for each case and burnup point. To get a single RPP, the [

]

[ ]

Eq. 4-8

It is noted that [

]

The power profiles are normalized such that ring area weighted average is unity (i.e., average pellet LHGR is equal to 1). This is needed so that the RPP value in each ring can be multiplied by the pellet power density and the area of the ring to obtain the LHGR of the ring. The ring powers from the selected [ ] RPP are therefore each divided by the area weighted average power of all rings.

The [ ] calculated results and RPP selection process is illustrated in Figure 4-5 through Figure 4-7 for 10 wt% enrichment, 6.0 wt% Gadolinia concentration, and 40% coolant void. In Figure 4-5, the K-value is plotted for each location and [

]

[

]

An illustration of the RPP at beginning of life and at 50 GWd/MTU pellet-average exposure is shown for the same case in Figure 4-6 and Figure 4-7, respectively.

Though the RPP is [

]

Figure 4-5
ATRIUM 11 K-values for 10.0% U-235, 6.0% Gad and 40% Void

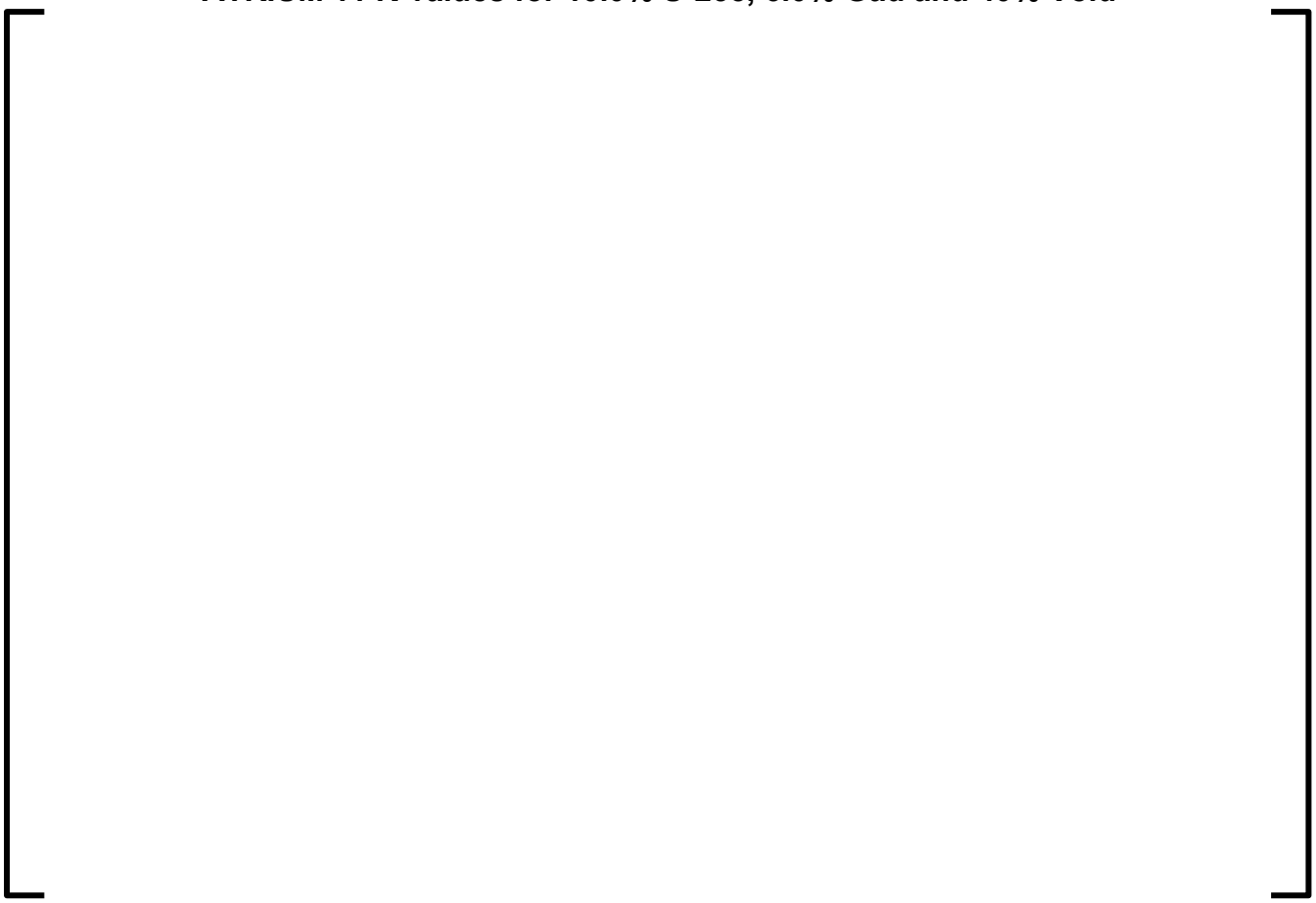

Figure 4-6
ATRIUM 11 RPPs for 10.0% U-235, 6.0% Gad, and 40% Void at Beginning of Life

Figure 4-7
ATRIUM 11 RPPs for 10.0% U-235, 6.0% Gad, and 40% Void at 50 GWd/MTU Pellet Exposure

EXAMPLES OF VERIFICATION OF THE IMPLEMENTATION IN RODEX4 OF THE [ ] RPP TABLES

Figure 4-8 through Figure 4-10 below illustrate the correct implementation of the [ ] Gadolinia tables, as well as examples of [ ] calculated RPPs. The default option for radial mesh in RODEX4 is 10 rings, but a finer mesh of 35 rings is also employed for determining highly nonlinear processes, such as High-Burnup Structure (HBS). This finer RPP data are also written in the main RODEX4 output file and can be overlayed on the 25 nodes [ ] RPP.

Due to differing exposure and radial meshes between RODEX4 and [ ] close but not identical RPP are expected for the test case; the small differences in the burnup and pellet radius of the test case from the [ ] tables were intended to verify the adequacy of the interpolation of the [ ] tables. Note that [ ] tables include 7% and 8.5% U-235, which straddle the 7.4% U-235 of the RODEX4 run [ ] It should be noted that, though the plots are overlayed, the RODEX4 RPP values are nodal values while the [ ] RPP values are ring averaged values.

Figure 4-8
Extended UGD tables verification for 7.4% U-235 and 8% Gd at 0 MWd/kgU exposure

Figure 4-9
Extended UGD tables verification for 7.4% U-235 and 8% Gd at 20 MWd/kgU exposure

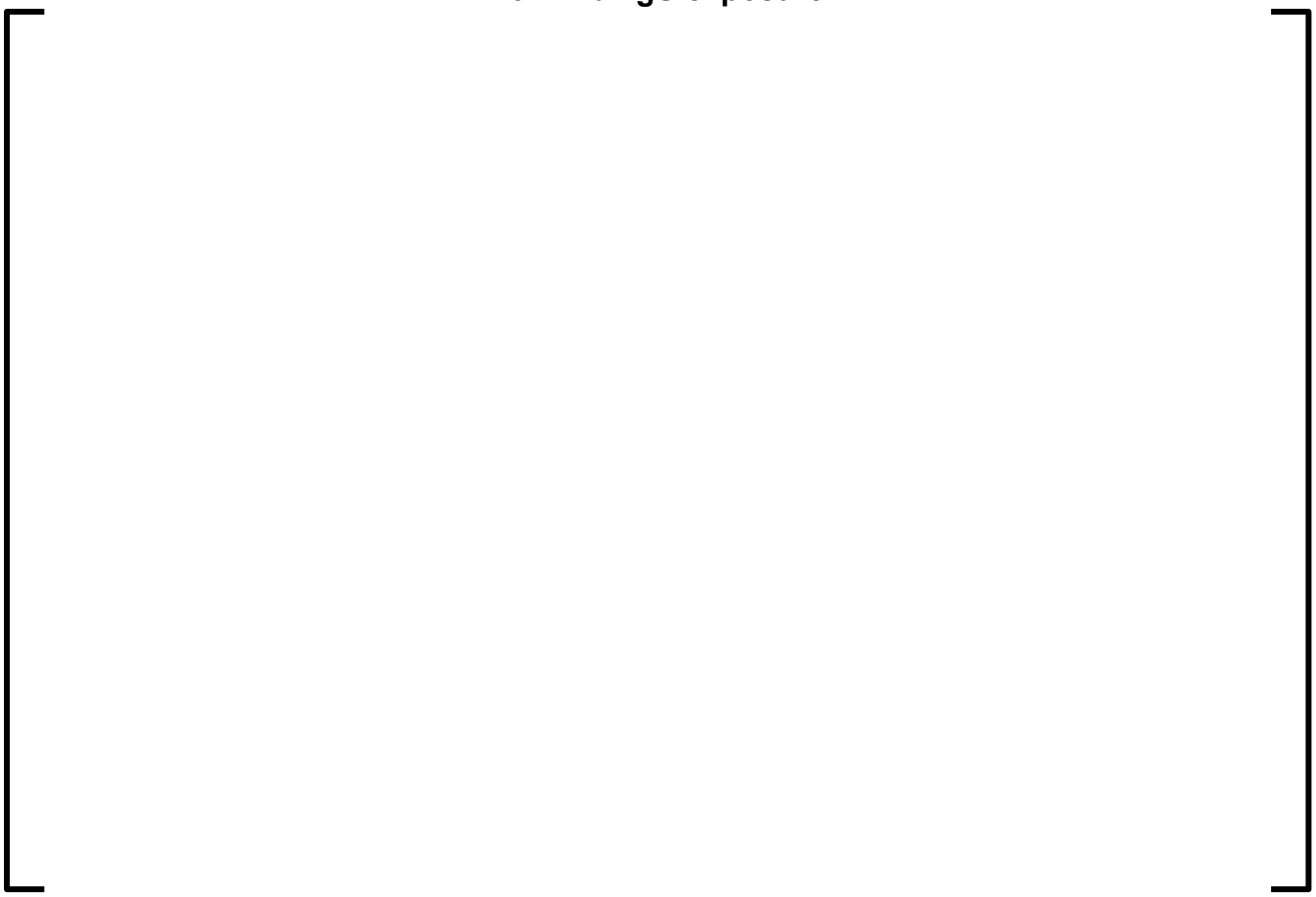

Figure 4-10
Extended UGD tables verification for 7.4% U-235 and 8% Gd at 70 MWd/kgU exposure

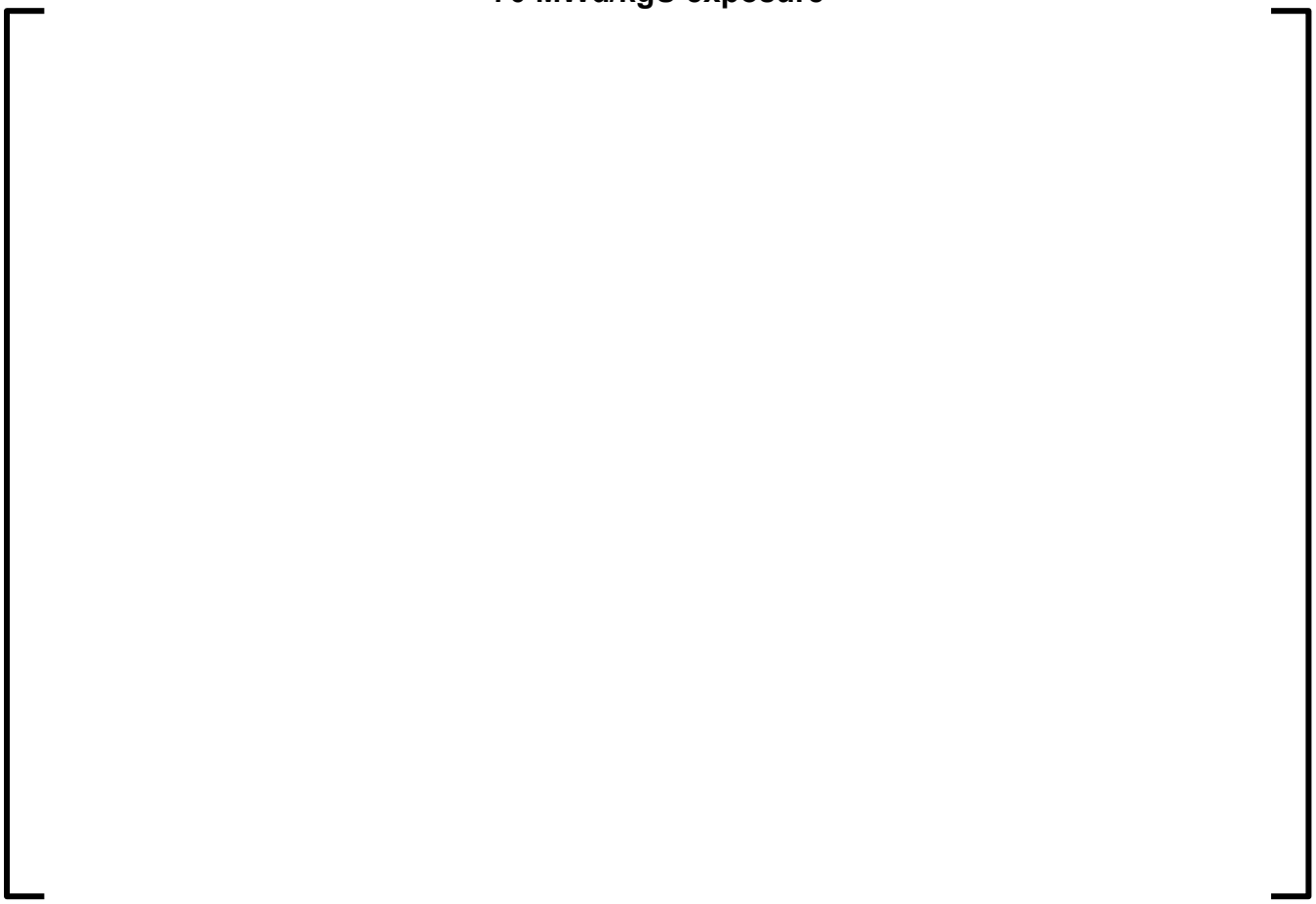

5.0 RAI 4

5.1 *RAI Text*

As stated in Section 6.1, "Dimensional Change," and Appendix B, "BWR Fuel Rod to Fuel Assembly Differential Growth Correlation," of TR BAW-10247, Revision 0, Supplement 3, the RODEX4 methodology for fuel rod growth has been revised to a differential fuel rod to fuel assembly growth model to evaluate the limiting end of life (EOL) margin. The burnup range of the fuel rod growth data shown in Figure B-2, "BWR Fuel Rod Growth Correlation for SRA Cladding," **[**

]. Framatome asserts NUREG-1475, Revision 1, “Applying Statistics,” was used in the extrapolation of these values to the burnup range requested. However, the statistical procedure used from NUREG-1475, Revision 1, within the TR is not entirely clear to the NRC staff. The statistical procedure used to develop the **[** **]** was described in more detail during the regulatory audit conducted from September 9, 2025, to September 11, 2025 (ADAMS Package Accession No. ML25212A128).

Therefore, the NRC staff requests that Framatome provide a discussion describing how the **[** **]** is applied within the fuel rod and fuel assembly growth model. Additionally, provide justification for extrapolating fuel rod/fuel assembly differential growth to higher burnup.

5.2 *RAI Response*

The NRC correctly reiterates that Framatome's methodology for evaluating fuel rod to fuel assembly upper tie plate engagement has been updated from using individual fuel rod and fuel assembly growth correlations to using a single fuel rod to fuel assembly differential growth correlation. Thus, Framatome is not seeking NRC approval for individual fuel rod and fuel assembly growth correlations such as those developed in Reference 17. The updated fuel rod growth and fuel assembly growth correlations [

]

The updated fuel rod growth curves were presented to the NRC during the regulatory audit conducted from September 9, 2025, to September 11, 2025 based on the latest available fuel rod growth data. The method for deriving the best estimate and UTL curves remains unchanged relative to that described in Reference 17 (Appendices B and C) and therefore does not utilize the methods described in [

] The updated UO_2 fuel rod growth curve, shown in Figure 5-1 remains applicable and conservative, particularly at high burnups where growth data tend to be well below prediction, and for modern designs which are consistently at the low end of the experience base. However, as discussed later, the methods described in [ ] were used for analysis of the fuel rod to fuel assembly differential growth correlation.

To further demonstrate the well-established behavior of SRA cladding material to high burnups, data exist which shows that relevant SRA materials exhibit stable and predictable behavior to irradiation doses well-exceeding the burnup limits requested here. High exposure stress-free irradiation growth experiments conducted in the BOR-60 test reactor (Reference 12) indicate that Zry-4 in the stress-relief annealed (SRA) condition exhibits a linear growth dependence versus exposure up to 33.7 dpa or 16.2 x 10^{25} n/m² (E >1 MeV) (Reference 12, Figure 14a), which roughly equates to an effective burnup of 96.6 MWd/kgU in a BWR environment, [

]

This conclusion is also supported by the Zry-2 RXA + 70% cold-worked specimen growth data (irradiated to the same exposures) also shown in Reference 12, Figure 14a. These data demonstrate that irradiation growth of Zry-2 SRA cladding up to the requested FA average exposure limit of [ ] is adequately represented by the [ ] presented in Figure 5-1.

Figure 5-1
Fuel Rod Growth Data Plotted Against Latest Fuel Rod Growth Best Estimate Curve. The Dataset is Identical to that Provided in Figure B-2 of Appendix B, but Plotted with More Discrete Data Series

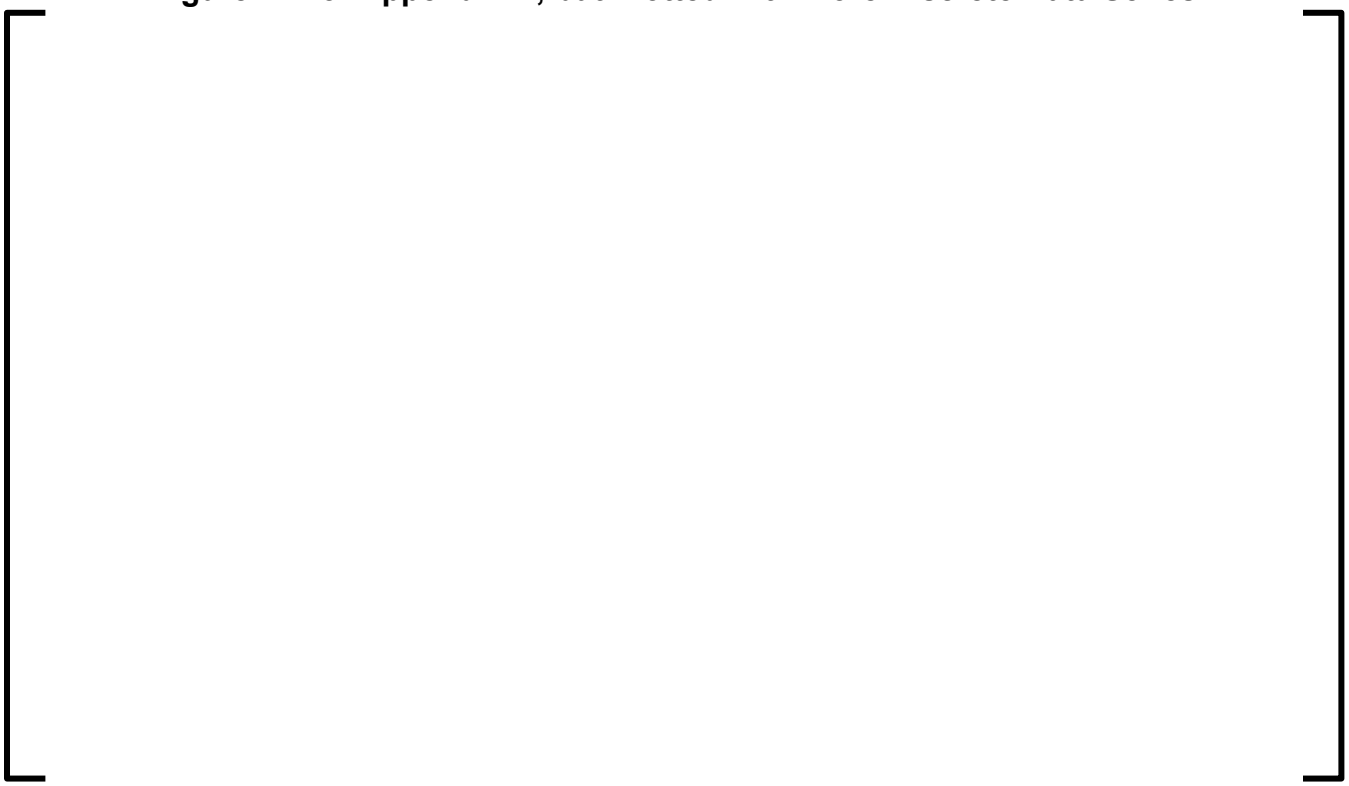

An RXA fuel rod growth dataset containing both UO_2 and chromia-doped fuel showing stable behavior well within prediction up to a fuel rod average burnup of **[ ]** is provided in Figure 5-2 and Figure B-5 of Appendix B of Reference 1. SRA fuel cladding is known to exhibit greater axial creep resistance and is therefore less susceptible to fuel swelling contributions to fuel rod growth. The combination of well-understood SRA material free irradiation growth behavior to an equivalent burnup of **[ ]** and well-behaved and understood UO_2 and chromia-doped pellet swelling / growth contributions in **[ ]** demonstrates that SRA fuel rod growth behavior to a FA average exposure of **[ ]** is well-understood and predictable.

Figure 5-2
UO_2 and Chromia-Doped RXA Fuel Rod Growth in BWR Reactor C22.
Data are Identical to Figure B-5 of Appendix B.

Justification for the extrapolation of the differential growth correlation to extended burnups begins with understanding the individual growth behaviors. Framatome SRA and RXA fuel rod growth behaviors were demonstrated in Figure 5-1 (similar to Figure B-2 of Appendix B) and Figure 5-2 (Figure B-5 of Appendix B), respectively, with a complete description and justification for fuel rod growth to the requested burnups given above. The complete fuel assembly growth database is shown below in Figure 5-3 and includes data up to [ ] fuel assembly average burnup and requires no extrapolation. Additionally, data from fuel channels (which have similar shape and composition to the water channels responsible for FA growth) indicate that the growth characteristics of fuel channels are well understood and modeled up to exposure values reaching about [ ] lending additional confidence in the FA growth correlation.

The differential growth correlation was developed using [

] This specific data set is shown below in Figure 5-4 and is [

] These data show that the updated individual fuel rod and fuel assembly design correlations represent the data conservatively, particularly at the higher burnup ranges.

Figure 5-3
Fuel Assembly Growth Database and Updated Best Fit Curve

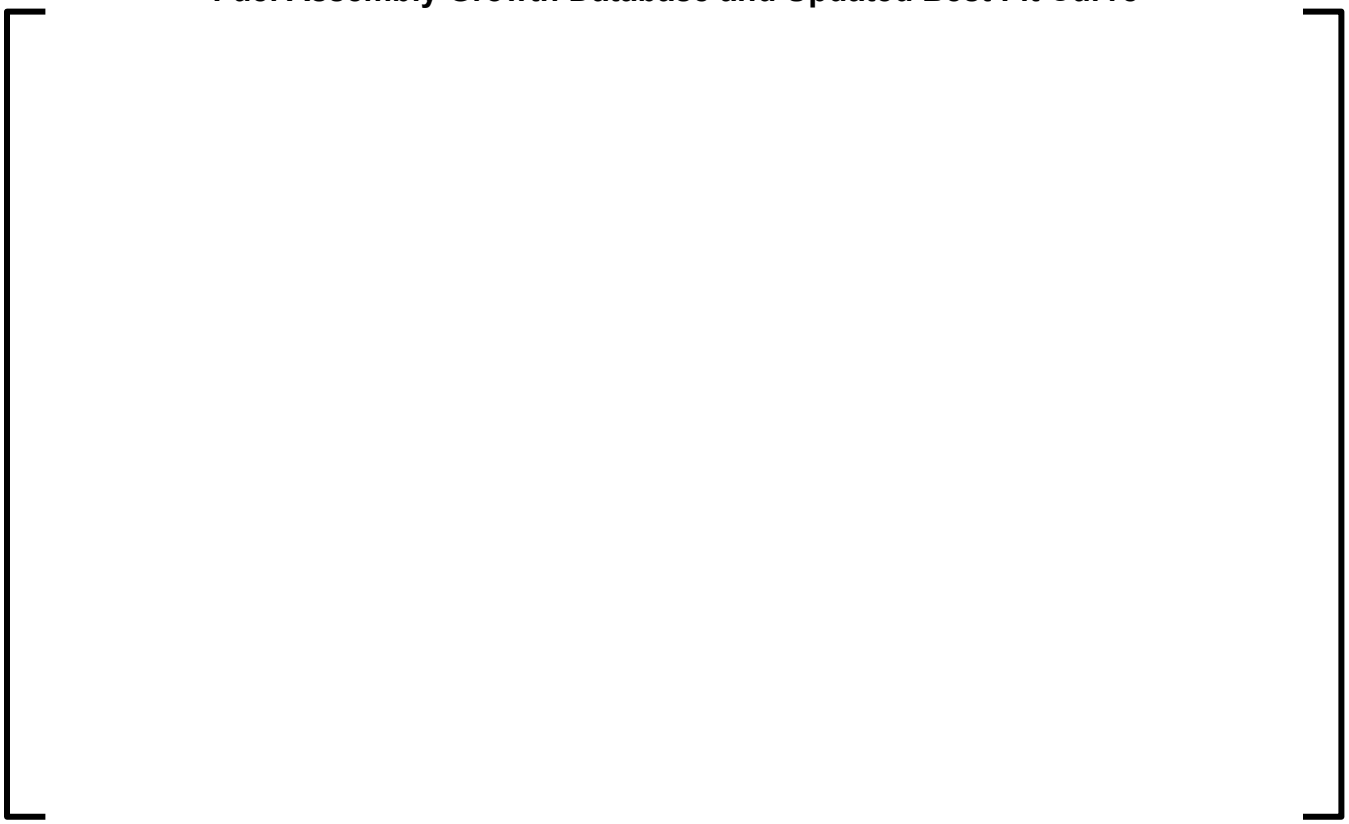

Figure 5-4
Fuel Rod Growth and Fuel Assembly Growth Data Used to Develop the Differential Growth Correlation

As differential growth is simply the difference between fuel rod growth [ ] and fuel assembly growth [ ] the resultant differential growth curve can be well described by [ ] as described in Appendix B. The data and associated design curves are shown in Figure 5-5.

Figure 5-5
UO_2 Differential Growth Data Overlayed with Design Curves. Data and UTL are Identical to Those Presented in Figure B-4 of Appendix B

Due to the need for extrapolation and desire to account for increased uncertainties in the extrapolated region, it was decided to employ the use of [ ] as described in [ ] and further described in Appendix B. [

]

[

] Eq. 5-1

]

Figure 5-6
UO_2 Fuel Rod-Fuel Assembly Differential Growth UTL relative to the [ ]

In addition to the conservative uncertainty treatment, there is a justified basis to conclude that collected data will remain within the existing UTL, particularly in the extrapolated range at higher burnups. There is observed trend and mechanistic reasoning showing that differential growth [

] These behaviors can be easily seen in Figure 5-1 and Figure 5-4.

The resulting differential growth, shown in Figure 5-5, demonstrates the [ ] To ensure conservative treatment at extended burnups, [

]

The combination of well-established and predictable fuel rod and fuel assembly growth behaviors to the requested fuel assembly burnup limit of [ ] combined with the conservative treatment of uncertainties used in the differential growth correlation, justifies the applicability of the fuel rod – fuel assembly differential growth correlation to a maximum fuel assembly burnup of [ ]

Clarifications for Update Process

The following is additional information in support of the revised update process included in this RAI response document. This information provides the justification of the increase or decrease limit in the UTL by one standard deviation for the rod bow correlation and UO_2 differential growth correlation, and the justification of [ ] limit for the chromia-doped differential growth UTL.

An increase or decrease of a correlation UTL by one standard deviation prior to resubmittal has become standard practice as it has been approved by the NRC as appropriate in several topical reports. It was discussed with the NRC during the submittal of EMF-93-177(P), Revision 1 in 2005 (Reference 13), that there have been several instances of Framatome receiving NRC approval for use of the "one standard deviation" resubmittal criterion. These include References 14 through 16 as well as in RODEX4, Supplement 2 (Reference 17) as discussed below.

1. In relation to Reference 14, discussing the fuel rod and fuel assembly growth correlations:

   "[…] SPC will resubmit the correlation for review and approval, if the correlation predictions change more than one standard deviation from those shown on the curve in the figure in the attachment due to the inclusion of new data in the correlation. Otherwise, the justification for application will continue to be submitted for each new fuel design as required by the Reference 1 topical report."

2. In relation to Reference 15, Attachment A, Framatome stated:

   "As new data becomes available, the correlation may be updated. If the correlation fits **[ ]** or if the form of the fitting equation is changed, SPC will submit the revised correlation to the NRC for review and approval. Likewise, the other growth correlations presented in this report will be resubmitted under the same conditions."

3. In relation to Reference 16, the NRC technical evaluation report of axial irradiation growth (Section 2.6) states:

   "If either the upper or lower bounds of the new axial growth model change by more than a standard deviation from the upper or lower bounds of the base axial growth model in Reference 5 the new model is required to be submitted to NRC for review."

4. In relation to Reference 17, NRC Limitations and Conditions 6 in the Final Safety Evaluation states:

   "Using the same method as described in the response to RAI 2, new upper or lower limits supported by database updates must be calculated. If the new limits are outside the envelope defined by the approved limits plus or minus one standard deviation, a new correlation must be submitted to the NRC for review and approval."

Therefore, the "one standard deviation" resubmittal criterion can be considered a generally accepted limit for acceptable changes to approved correlations without requiring NRC review.

With respect to the rod bow and UO_2 differential growth correlations, the term 'standard deviation' is used colloquially to demonstrate the practical similarity with existing standard practices. More specifically, the rod bow and UO_2 differential growth UTLs may increase or decrease by [

] Use of [

] is consistent with the generation of the uncertainty intervals, including the [ ] derived for the UO_2 differential growth correlation. Given the above description, [

]

Although the chromia-doped [

] is once again used colloquially to demonstrate the practical similarities with existing standard practices. As stated earlier in this RAI response, [

] To avoid confusion in terminology, [

]

[

] reasonable upper and lower change limits can still be obtained by applying [

] The stated change limits for the chromia-doped differential growth UTL ensure limited and reasonable updates are possible while setting conservative thresholds when the correlation must be resubmitted for approval.

Figure 5-7
UO_2 and Chromia-Doped Differential Growth UTL Change Limits Relative to (Effective) Standard Deviation

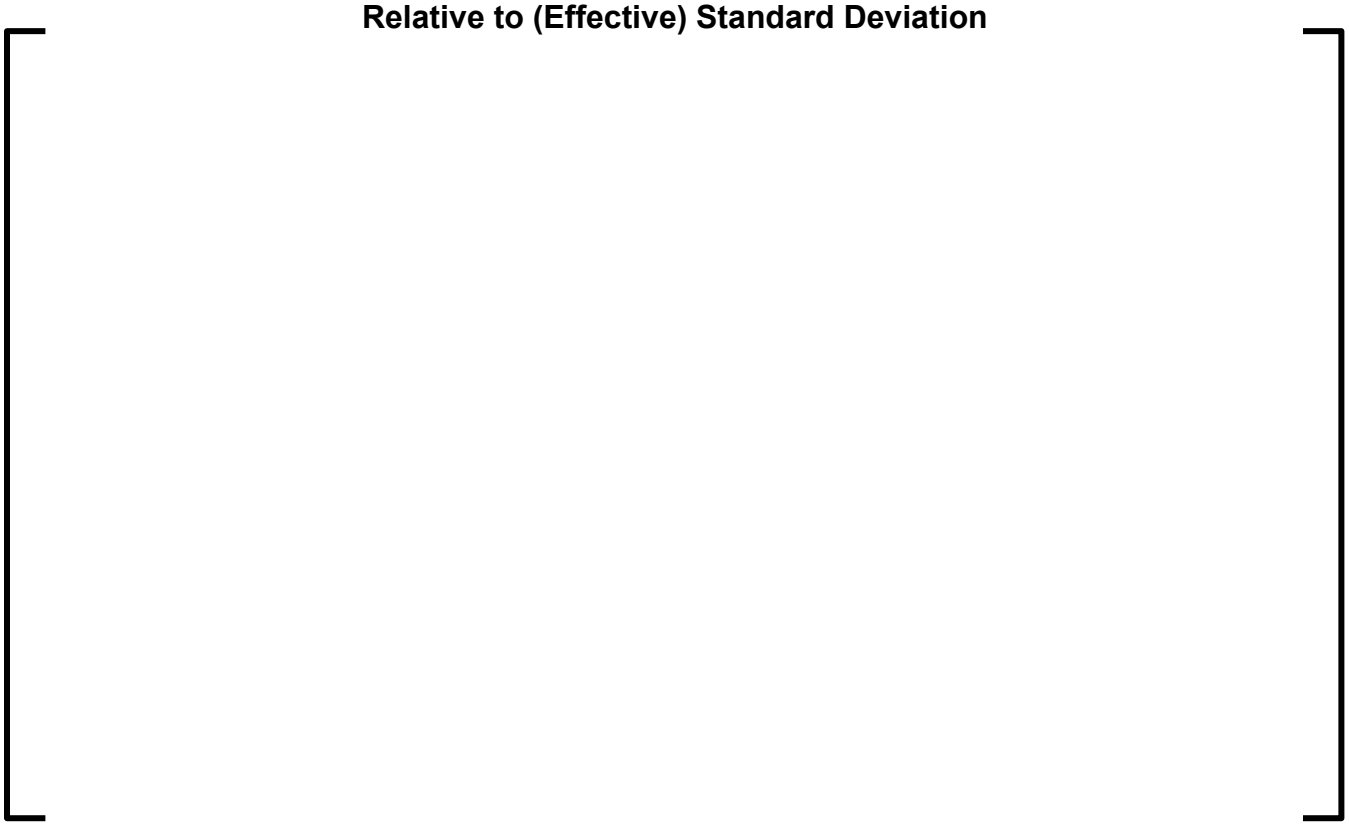

6.0 RAI 5

6.1 *RAI Text*

Line A.V of Table 2-1, "Standard Review Plan Section 4.2 Criteria," of TR BAW-10247, Revision 0, Supplement 3 states that the previously approved channel bow method (TR BAW-10247Q3(P), Appendix B (ADAMS Package Accession No. ML081340220)) [

] However, no justification is provided within the TR to support this assertion. Additionally, while BAW-10247Q3(P), Appendix B, provides a discussion on the determination of [

] no discussion is provided in BAW-10247Q3(P), Appendix B, or the current TR regarding the applicability of the approach for [

] or assurances that the resulting [

]

will yield results that remain within the approved [ ] of RODEX4.

The NRC staff requests that Framatome provide justification that the previously approved channel bow method discussed in BAW-10247Q3(P), Appendix B, [

] for RODEX4. Additionally, provide justification [

] currently approved for RODEX4 as specified in Section B.7 of BAW-10247Q3(P), Appendix B.

6.2 *RAI Response*

A mechanistic model for channel bow is described in Section B.4 of BAW-10247Q3(P), Appendix B. Channel bow is the result of uneven axial deformation of the two pairs of parallel, opposite channel walls. This differential growth of channel sides is caused by differential stress-free irradiation growth strain of the opposite channel sides as a result of differences in the fast neutron fluence of the respective channel opposite sides. Obtaining channel bow given the stress-free irradiation growth strain in each channel wall is described geometrically and [

]

In Section B.5 of BAW-10247Q3(P), Appendix B, a correlation is presented to compute stress-free irradiation growth axial strain [

]

It remains to verify [

]

[

]

The ARTEMIS-B steady state core simulator was reviewed and approved by the NRC in Reference 3. [

]

A plot of the calculated channel bow versus the measured channel bow is given in Figure 6-1. [

]

Table 6-1
Channel Bow Benchmark Results

[

]

Figure 6-1
Combined Data Set, ARTEMIS-B and MICROBURN-B2 Calculated versus Measured Channel Bow

7.0 RAI 6

7.1 *RAI Text*

In Section 3.2.2, "G6-Cladding Mechanical Properties," of TR BAW-10247, Revision 0, Supplement 3, Framatome provides Figures 3-9, "Mechanical Testing on Irradiated Cladding," and 3-10, "Burst Strains for Irradiated Cladding, Hydrogen < 500 PPM." These figures encompass data from various mechanical tests which respectively demonstrate that the irradiation hardening of fuel rod cladding saturates around the midlife of fuel rods, and that the irradiated cladding continues to satisfy the one percent uniform strain licensing criterion under the effects of hydrogen and irradiation embrittlement through EOL. Framatome asserts that these conclusions from the mechanical tests indicate that RODEX4 can calculate stress and strain at higher burnup levels. The figures provided are comprised strictly of datasets, which do demonstrate Framatome’s claim that the mechanical parameters remain consistent while approaching EOL, but no predictive capability of RODEX4 is shown. Because only data is provided, the figures do not adequately demonstrate RODEX4’s ability to adequately capture the saturation effect shown in the data, and in turn, accurately and reliably predict the mechanical parameters at higher burnup.

Therefore, the NRC staff requests that Framatome provide a comparison of RODEX4’s calculations of yield stress and plastic strain over the range of fast neutron fluence to the datasets shown in Figures 3-9 and 3-10 (i.e., a calculated vs measured plot vs fluence for what is shown in Figures 3.9 and 3.10).

7.2 *RAI Response*

The cladding mechanical model in RODEX4 is a unified visco-plastic model that allows modeling both the so-called plastic deformation (assumed to be instantaneous in plasticity theory) and creep deformation with the same phenomenological model; the difference between plastic and creep deformations is the strain rate at which they occur, being very large for the former and moderate to lower for the latter. The generalized strain rate constitutive equation is implemented within the framework of a 3D Levy-Von Mises flow equations and Hill's anisotropy formalism. Therefore, all multiaxial loading conditions, as well as particular cases, such as uniaxial and biaxial internally pressurized closed tubes can be adequately modeled.

The role of the cladding mechanical model in modeling fuel rod behavior is to adequately calculate cladding deformation, so that the feedback with the other fuel rod processes is correctly evaluated. Also, compliance with the one percent (1%) hoop strain licensing criterion is one of the main objectives of fuel code modeling. The failure strain is not necessary for design and licensing calculations and there is no mechanical failure model in RODEX4, because the 1% hoop strain criterion is used to conservatively estimate mechanical failure.

The stress alongside strain is a main variable of the cladding mechanical model and the evolution of the yield stress with irradiation was analyzed by performing mechanical tests on irradiated cladding. The cladding strain under neutron flux and after irradiation by mechanical tests provides data to calibrate and validate cladding mechanical model.

The following sections describe the results of this verification and validation of stress and strain data for RODEX4. As explained above, RODEX4 does not have a mechanical failure predictive model, so that the failure strains plotted in Figure 3-10 of the Supplement 3 topical report (Reference 1) cannot be benchmarked. However, simulation of mechanical tests Framatome performed on high burnup fuel rods will be summarized below to demonstrate that the RODEX4 mechanical model agrees with experimental strain-stress data and that the 1% strain criterion is met by the data.

YIELD STRESS

The yield stress calculation based on RODEX4 mechanical model of the cladding was described in the Supplement 1 RODEX4 topical report (Reference 8). The full derivation is not repeated here, only the final formula and the elements of the calculation of the uniaxial yield stress, Y_z, are summarized as follows.

The uniaxial tensile test is characterized by only the axial stress being different from zero. The axial yield stress, Y_z, is estimated by using a strain rate of 0.5% min^{-1}, which is the ASTM recommended value that is typically used in tensile tests. The permanent strain is set to 0.2%, which is the definition for the yield stress. Then, by inverting the hyperbolic sinh function, a relation is obtained for the axial yield stress.

[ ] Eq. 7-1

Where,

[ ] Eq. 7-2

and A_{zbt} and A_{zat} are constants related to material anistropy. The denominator of Eq. 7-1 contains the H_y factor, which accounts for irradiation hardening according to the following formula, in which Ψ is the fast fluence (greater than 1 MeV) :

[ ] Eq. 7-3

In the case of internally pressurized, burst tests, the biaxial yield stress is converted to uniaxial yield stress by using the following relation:

[ ] Eq. 7-4

where, R and P are the anistropy parameters.

The evolution with fast fluence of the uniaxial yield stress for SRA (SR) and RXA (RX) metallurgical condition of Zry-4 and Zry-2, respectively was calculated according to and overlaid as dashed lines on Figure 3-9 of (Reference 1), as shown below in Figure 7-1. It is noted that the full lines of the original figure are not fitted or calculated but rather just hand drawn to illustrate the irradiation hardening caused increase in yield stress with irradiation (see Figure 7-1). Also, the datapoints shown in the figure come from different materials with different fabrication parameters, which is illustrated by the large range of the yield stress in unirradiated condition (see legend and datapoints at zero fast fluence). This makes the estimation of delta stress between irradiated and non-irradiated yield stresses less accurate at low fast fluences.

Figure 7-1
Calculated yield stress increase with irradiation overlayed on mechanical test data

The apparent difference in the calculated delta yield stresses and the trend lines of the original figure is addressed by the more recent Framatome program of mechanical tests on irradiated Zry-2 cladding in the RX condition. The results were included in the Supplement 1 RODEX4 topical report (Reference 8) and a contemporaneous TopFuel paper (Reference 9), showing compliance with the 1% strain criterion for the samples from cladding irradiated to fast fluences between 2E+21 and 9E+21 n/cm^2, E > 1 MeV. The figure showing the uniaxial yield stress is reproduced from Supplement 1 (Reference 8) as Figure 7-2. It is noted that this figure contains prior uniaxial yield stress data up to 12 n/cm^2, E > 1 MeV, as well as data from an older [ ] test program (RX, but different manufacturing parameters).

Figure 7-2 illustrates the variation of the absolute yield stress with irradiation, but it can be seen that the yield stress increment saturates at [ ] in accord with the value indicated in Figure 7-1. Moreover, the expanded fast fluence range of Figure 7-2 confirms the leveling off of the yield stress, which is practically constant at high burnup, including the extended burnup range for which application of RODEX4 is demonstrated in the Supplement 3 RODEX4 topical report (Reference 1).

Figure 7-2
Variation of RX Zry-2 yield stress with irradiation

RECENT BURST AND HARDENING/RELAXATION TESTS

Recent mechanical tests on irradiated cladding have been performed on fuel rods fabricated by Framatome Inc and irradiated in a BWR-4 reactor to a fast fluence of around [ ] n/cm^2, E > 1 MeV (Reference 10).

A specially designed apparatus was used to perform both burst tests and Hardening Relaxation (HRX) tests. In the burst tests internal specimen pressurization was varied to achieve a prescribed strain rate until failure. In the HRX tests, loading of the specimen continued until a prescribed strain (greater than 1%) was reached after which the hoop stress was maintained at a constant value for a certain hold time to allow strain relaxation (conversion of elastic strain to plastic strain). The strain was measured online by two gauges at fixed locations, denoted EX13 and EX24.

Figure 7-3 through Figure 7-6 illustrate the calculations and experimental data for burst tests on RX and SR Zry-2 cladding specimens, while Figure 7-7 shows stress/strain evolution for an HRX test on SR Zry-2 cladding. The good agreement between calculation and measured stress and strain demonstrates that the evolution of stress and strain for irradiated cladding is adequately captured by the model, and both the yield stress and plastic strain are well predicted by the RODEX4 cladding mechanical model.

Figure 7-3
Burst test of RX Zry-2 cladding at 300°C

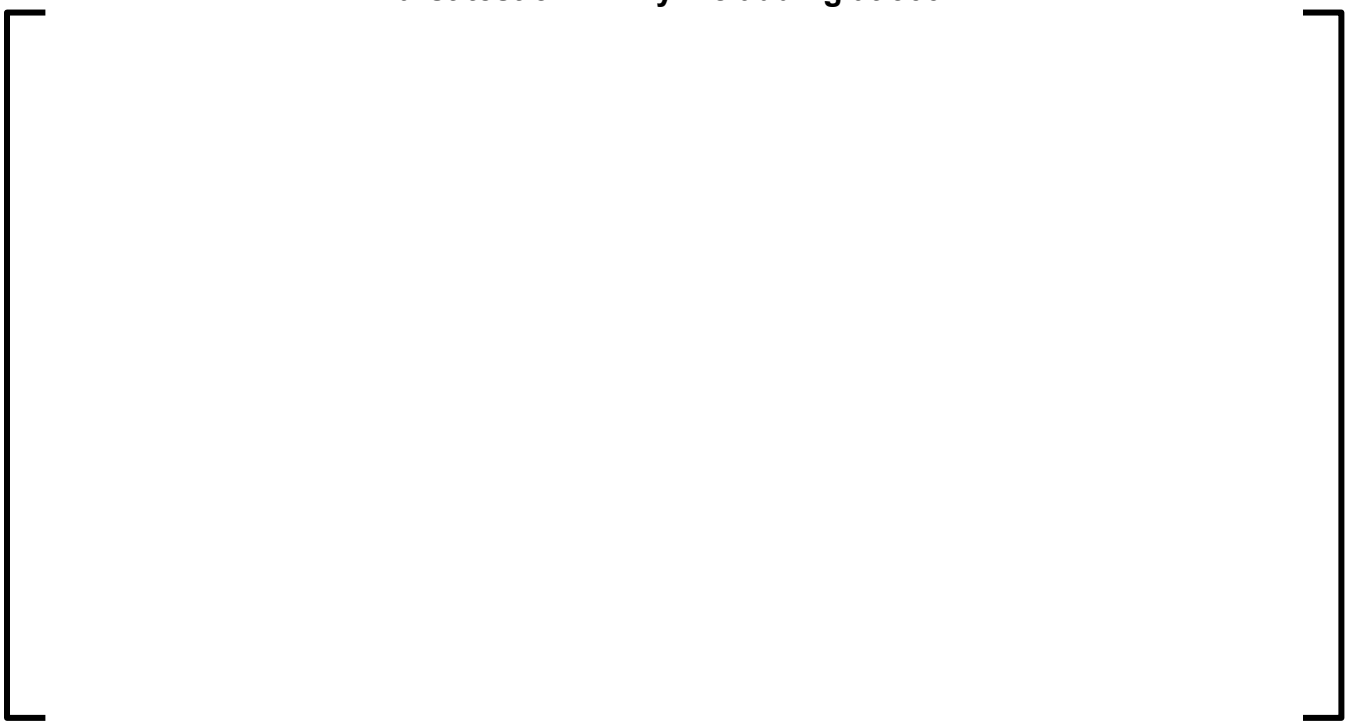

Figure 7-4
Burst test of SR Zry-2 cladding at 120°C

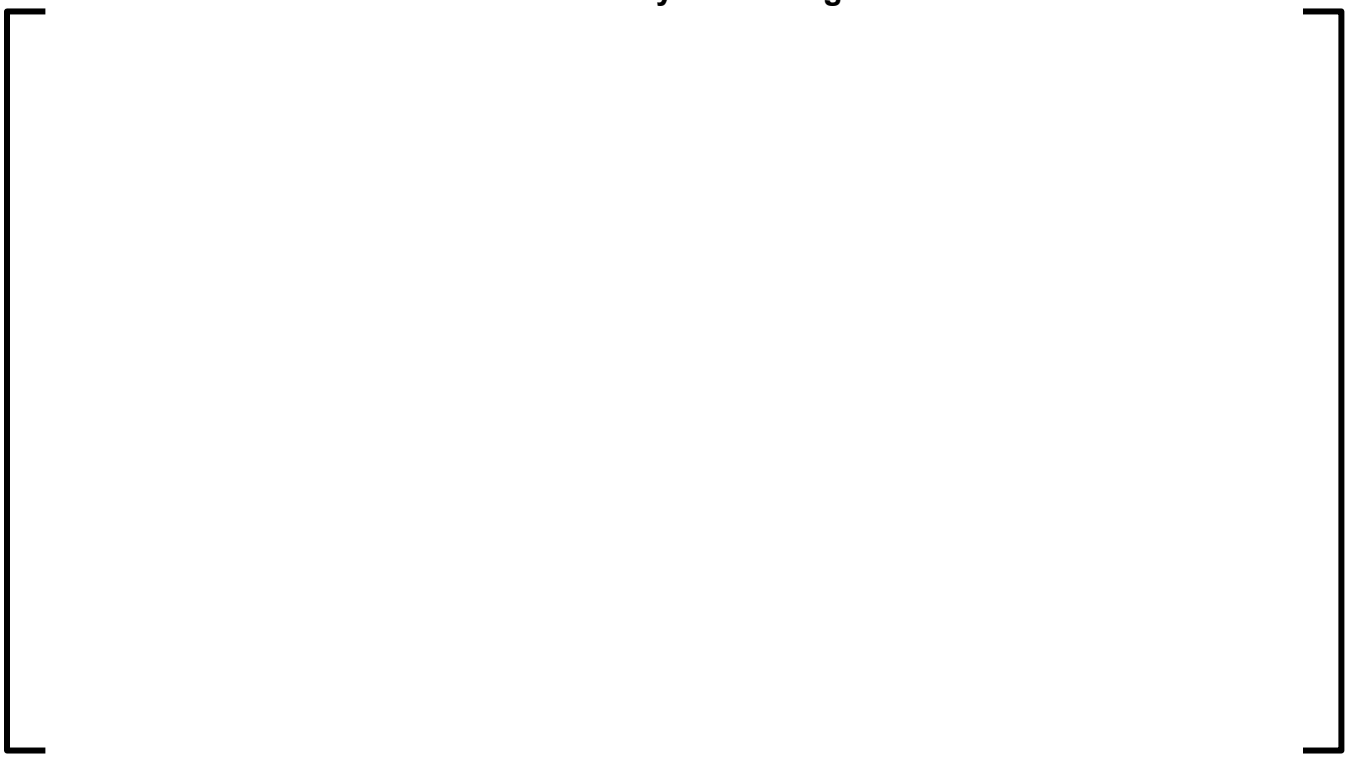

Figure 7-5
Burst test of SR Zry-2 cladding at 300°C

Figure 7-6
Burst test of SR Zry-2 cladding at 350°C

Figure 7-7
HRX test on SR Zry-2 cladding at 300°C

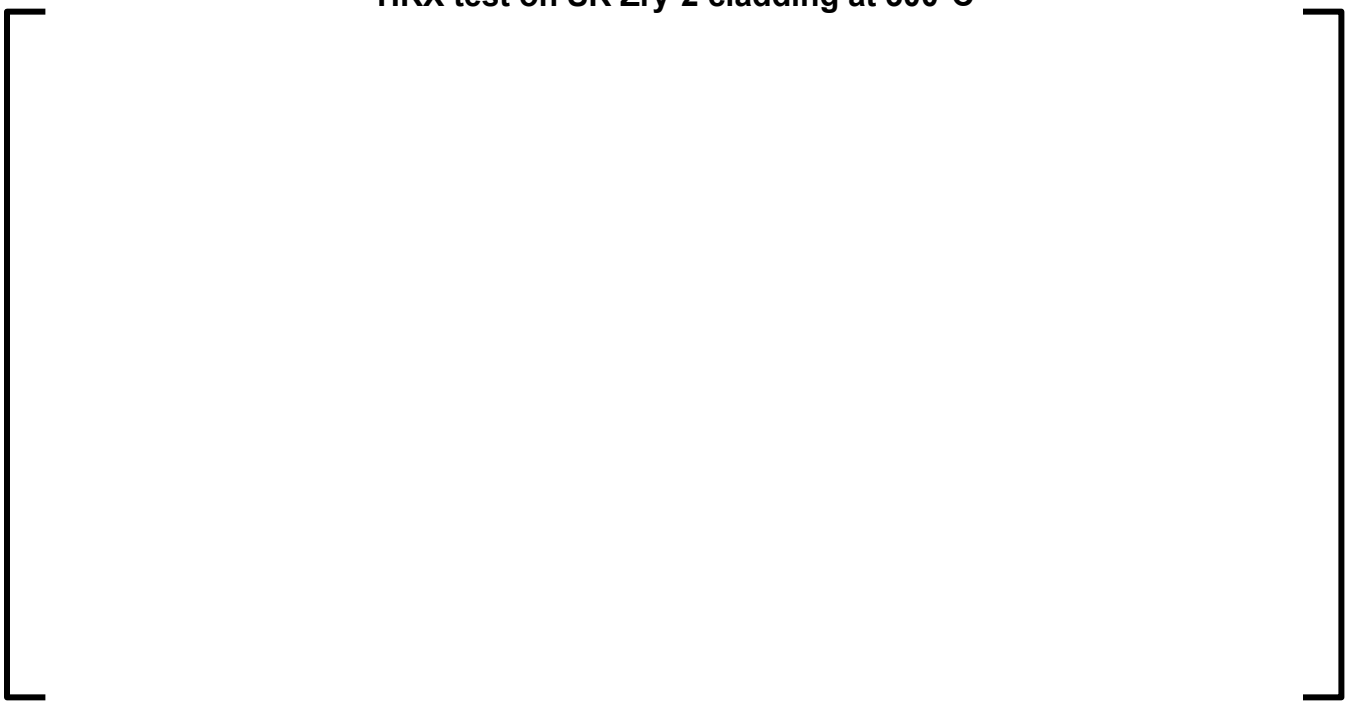

CLADDING PLASTIC STRAIN DURING STEADY STATE IRRADIATION AND TRANSIENT OPERATING CONDITIONS

The RODEX4 cladding mechanical model calculations of cladding deformation were verified and validated over the exposure range (and associated fast fluences) available in the database, which extends up to [ ] Both steady-state and transient strain increment experimental data have been benchmarked and best-estimate prediction has been demonstrated (details are available in the original topical report (Reference 6) and the RODEX4 Verification and Validation Report (Reference 11)).

Of particular interest is the power ramp strain increment case Mark-BEB at [ ] The post-ramp hoop strain increment for the three rods of the Mark-BEB case was greater than 1%, ([ ] as shown in the RODEX4 V&V Report (Reference 11, Figure 7.7)); this is conservatively exceeding the 1% strain licensing limit, which is the sum of elastic and permanent (plastic and creep) strains. Additional plastic strain data are available from the recent Framatome mechanical tests presented in the previous section.

Converting the burnup to the fast fluence E > 0.82 MeV used in Figure 3-10 of the Supplement 3 topical report (Reference 1), the [ ] and the recent mechanical test data are overlayed as bars on Figure 3-10, as shown in Figure 7-8 below. Note that the [ ] datapoints are for non-failed fuel rods so that the failure strain value is larger than shown by the respective bar. Figure 7-8 shows that the recent plastic strain data are consistent with the data of the original Figure 3-10 of the Supplement 3 topical report. Moreover, the recent plastic strain data are at the upper bound of the fast fluence range of Figure 3-10 and thus confirms the applicability of the RODEX4 cladding mechanical model to the extended burnup range by taking into account the saturation of irradiation hardening, as illustrated by the leveling off of the yield stress in Figure 7-1 and Figure 7-2.

Figure 7-8
Calculated plastic strain increments overlayed on
Figure 3-10 of Reference 1

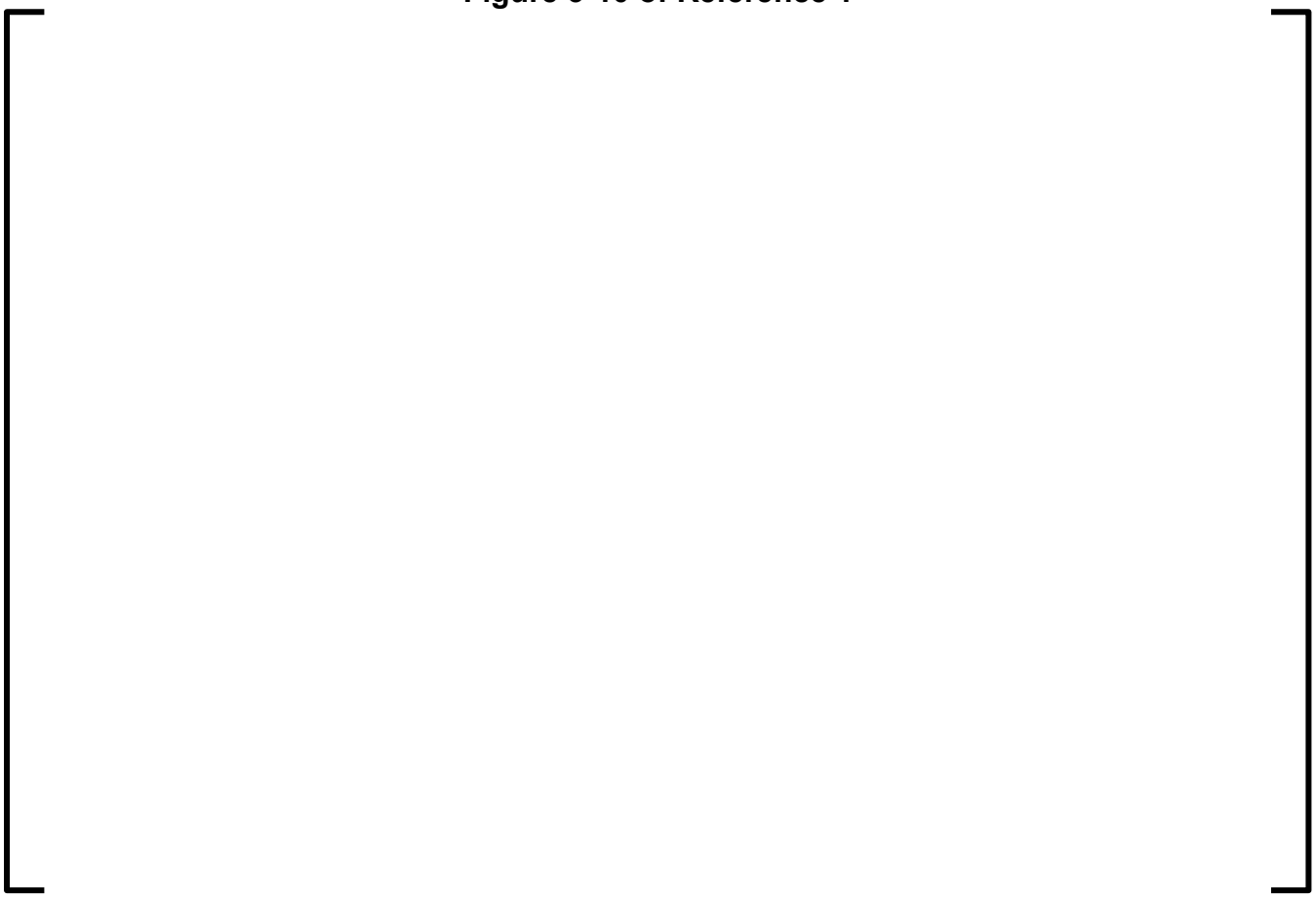

8.0 REFERENCES

1. BAW-10247P, Revision 0, Supplement 3, Revision 0, “Realistic Thermal-Mechanical Fuel Rod Methodology for Boiling Water Reactors, Supplement 3: Extension to Higher Exposures,” April 2025.
2. Email, Ngola Otto (NRC) to Alan Meginnis (Framatome Inc.), “Request for Additional Information-11050, Topical Report, BAW-10247, Revision 0, ‘Realistic Thermal-Mechanical Fuel Rod Methodology for Boiling Water Reactors, Supplement 3: Extension to Higher Exposures’,” NRC Accession Number ML25343A23, December 16, 2025.
3. ANP-10350P-A, Revision 0, “Framatome Methodology for Boiling Water Reactors: Evaluation and Validation of APOLLO2A-/ARTEMIS-B,” July 2025.
4. BAW-10247PA, Revision 0, “Realistic Thermal-Mechanical Fuel Rod Methodology for Boiling Water Reactors,” February 2008.
5. ANP-10340P-A, Revision 0, “Incorporation of Chromia-Doped Fuel Properties in AREVA Approved Methods,” May 2018.
6. ANP-10350P, Q4P, Revision 0, “Framatome Methodology for Boiling Water Reactors: Evaluation and Validation of APOLLO2-A/ARTEMIS-B,” October 2024.
7. ORNL/TM-2020/1833, “Isotopic and Fuel Lattice Parameter Trends in Extended Enrichment and Higher Burnup LWR Fuel,” Vol. 1, PWR Fuel, NRC Accession Number ML21088A336.
8. BAW-10247PA, Revision 0, Supplement 1P-A, Revision 0, “Realistic Thermal-Mechanical Fuel Rod Methodology for Boiling Water Reactors, Supplement 1: Qualification for RODEX4 for Recrystallized Zircaloy2 Cladding,” April 2017.
9. Arimescu, I., Goll, W., and Hoffmann, P. B., “Recrystallized Zircaloy-2 Mechanical Properties After Irradiation and Associated H Pickup,” Topfuel, 2013.

10. Mon, K., Arimescu, I., and Beale, J., “Mechanical Effects of Hydrogen on Cladding Material: Results of a Hot Cell Investigation,” Topfuel, 2025.

11. EMF-3014, Revision 0, “RODEX4: Thermal-Mechanical Fuel Rod Performance Code Verification and Validation Report,” August 2004.

12. Yagnik, S., Adamson, R. B., Kobylyansky, G., Chen, J.-H., Gilbon, D., Ishimoto, S., Fukuda, T., Hallstadius, L., Obukhov, A. and Mahmood, S., “Effect of Alloying Elements, Cold Work, and Hydrogen on the Irradiation-Induced Growth Behavior of Zirconium Alloy Variants,” Zirconium in the Nuclear Industry: 18th International Symposium, ASTM STP 1597, R. J. Comstock and A. T. Motta, Eds., ASTM International, West Conshohocken, PA, 2018, pp. 748-795.

13. Additional Information - EMF-93-177(P) Revision 1, "Mechanical Design for BWR Fuel Channels," NRC Accession Number ML051160269, 2005.

14. Letter, H. Donald Curet (SPC), to NRC Document Control Desk, "ATRIUM-10 Irradiation Growth Evaluation," HDC:97:0019, NRC Accession Number ML20135C993, February 1997.

15. EMF-85-74(P), Revision 0, Supplement 1(P)(A) and Supplement 2(P)(A), “RODEX2A (BWR) Fuel Rod Thermal-Mechanical Evaluation Models” February 1998.

16. EMF-92-116(P)(A), Revision 0, “Generic Mechanical Design Criteria for PWR Fuel Designs” Siemens Power Corporation, NRC Accession Number ML003681173, February 1999.

17. BAW-10247P-A, Supplement 2P-A, Revision 0, “Realistic Thermal-Mechanical Fuel Rod Methodology for Boiling Water Reactors Supplement 2: Mechanical Methods,” August 2018.

APPENDIX A: MARKUP PAGES

Table A-1
Markup Pages and Changes

New Page Number	Original Page Number	Description of Change
1-2	1-2	Corrected “develop” to “developed”.
2-7	2-7	Add “rod” to obtain “fuel rod” for clarification.
2-10	2-10	Corrected spelling of “applicable”.
3-1	3-1	Corrected spelling of “experience”.
3-11	3-11	Corrected “Figure 3-4” to “Figure 3-6”.
3-20	3-20	Improved readability of equation.
3-24	3-24	Corrected “RXS” to “RXA”.
4-1	4-1	Corrected “RAI” to “RIA” in subsection title.
5-1	5-1	Changed “they” to “the new model is” for clarity.
5-2	5-2	Corrected “updated versions” to “updated version”.
7-1 through 7-5	7-1 through 7-2	Upper and lower change limits are specified for the chromia-doped differential growth correlation UTLs. Allowance for RODEX4 changes has been removed. Reference to design criteria for changes has therefore been removed. Section 7 has been rewritten for improved clarity. Additional information is provided at the end of RAI 4 response.
9-2	9-2	Made corrections as follows: Added “-A”, changed “Revision 0” to “Revision 1” to citation of Reference 10 and changed issuance date to “January 2018”. Added “-A” to citation for Reference 11 and changed issuance date to “March 2019”. Added “-A” to citation for Reference 12 and changed issuance date to “March 2018.”
A-2	A-2	Corrected **[ ]**
B-1	B-1	Corrected “Figure B-1” to “Figure B-2”.
B-2	B-2	Corrected “Figure B-3 show” to “Figure B-3 shows”.
B-2	B-2	Changed “measurement” to “growth measurements” for clarity.

New Page Number	Original Page Number	Description of Change
B-5	B-5	Clarified precision and use of chromia-doped fuel enhancement factor consistent with update process documented in Section 7.
B-7	B-7	Corrected title of Figure B-2, replacing "Correlation" with "Data".
B-8	B-8	Updated plot in Figure B-3 by removing redundant legend entry for conciseness.
B-9	B-9	Corrected plot in Figure B-4 as reported during audit.

List of Tables

List of Figures

Section 4.0 provides discussions of phenomena that are not represented in the RODEX4 methodology but are relevant to its application.

Section 5.0 discusses the modest changes to the encoded RODEX4 methodology in the RODEX4 computer code to support the higher exposures. Also included is a description of the implementation of an already approved methodology for a new hydrogen uptake model and an improved cladding corrosion model. This section also includes a summary description of a sample problem illustrating the application of the RODEX4 code to a nuclear fuel cycle design with higher exposures. The details of the sample problem are provided in Appendix A.

Section 6.0 contains aspects of the RODEX4 methodology beyond that embodied in the RODEX4 code and which address modeling of the fuel rods and fuel assembly components and the interactions of both.

Section 7.0 discusses how the methodology will be updated when relevant new data is obtained.

Finally, Section 8.0 describes the Framatome Quality Assurance Program under which methodology is developed and applied.

2.2 *Prior Submittals of the RODEX4 Methodology*

The original RODEX4 Methodology is documented in Reference 1. It is a best-estimate methodology to analyze the performance of BWR fuel rods and is comprised of three parts as illustrated in Figure 2-1. These are a foundational Fuel Performance Database that spans the range of parameters important to BWR fuel rod thermal-mechanical performance and provides the theoretical underpinnings for the models and correlations used in the methodology, a best-estimate computer code, RODEX4, that embodies those models and correlations, and an application methodology that provides the non-parametric order statistics framework for the application of the methodology to batches of BWR reload fuel. The Phenomena Identification and Ranking Table (PIRT) from the original submittal remains applicable to extended exposures.

The original methodology was approved for exposures up to a full-length fuel rod-average exposure of 62 MWd/kgU. The neutronics methodology supporting the power histories required for RODEX4 analyses were limited to an enrichment of 5 wt% U-235.

The methodology has been extended in two supplemental topical reports. The first extension, that was documented in Reference 2, added models for Recrystallized Annealed zircaloy (RXA) cladding (the original submittal only included Stress-relieved Annealed (SRA) cladding), and a new cladding hydrogen pick-up model and cladding corrosion model. The second extension, that is documented in Reference 3, added several models and correlations for the mechanical analysis for BWR fuel assemblies that are not included in the thermal-mechanical analyses. There are: 1) a new BWR fuel rod bow correlation, 2) axial irradiation growth correlations for fuel rods and other fuel assembly components, and Z4B models and correlations for internal water channels. The fuel rod bow, and fuel rod and fuel assembly growth models were approved to a fuel assembly-averaged exposure of [ ]

For parameters for which additional information must be provided, the availability of Framatome proprietary data that supports exposure extension is provided in Section 3.0.

2.4 *Exposure Distributions in Part-length Fuel Rods*

In the original RODEX4 topical report (Reference 1), an exposure limit on fuel rods of 62 MWd/kgU was specified for full-length fuel rods. Due to the characteristics of BWR operation, the nodal exposures toward the top of a full-length fuel rod are usually less than the values toward the bottom of the same fuel rod. Since the part-length fuel rods are only present in the lower parts of the core, their fuel rod-average exposures may be higher than the limit imposed on full-length fuel rods. After the approval of the RODEX2A topical report, it was questioned whether the 62 MWd/kgU full-length fuel rod average exposure limit approved for the method should also apply to part-length fuel rods. To address the question Framatome (AREVA at that time) provided information to the NRC in two letters of clarification asserting that it would be inappropriate to apply the full-length fuel rod exposure limits to part-length fuel rods (References 16 and 17). The NRC responded with a letter concurring with the Framatome position (Reference 18).

The above position was deemed applicable for the original RODEX4 methodology. Similar supporting information was developed such that only a full-length fuel rod exposure limit was specified and approved in the topical report. The salient observations that support the position, and which continue to be valid for the RODEX4 methodology for analyses with exposures up to [ ] are as follows:

1. The nodal exposures for PLFRs are similar to, but typically lower than the nodal exposures of the FLFRs. If the nodal exposures of the FLFR is averaged over the axial elevations where the PLFR has fuel, then the corresponding average exposure for the FLFR is generally higher than that of the PLFR. (In these comparisons, the FLFR and PLFRs with the highest exposure values were compared.)

3.0 RODEX4 THERMAL-MECHANICAL APPLICABILTY TO EXTENDED EXPOSURE RANGE

A comprehensive review of Framatome's BWR high-exposure irradiation programs and operating experience is available in Reference 8. This reference contains a succint review of the evolution of the ATRIUM design for BWR fuel assemblies, which culminated with the current ATRIUM 11 product that is in operation in United States and Europe. A summary of operating experience in terms of fuel assembly end-of-life exposure and number of fuel assemblies/rods irradiated in commercial BWRs is presented in Table 1 of that paper, which is reproduced here as Table 3-1.

3.1.2.4 Application of RODEX4 FGR model to Cr-doped Fuel

Validation of fission gas release for Cr-doped fuel was achieved without making any change to the RODEX4 fission gas release model. That model accounts for grain size and therefore automatically captures the beneficial effect of larger grain size in retarding the gas atom diffusion to the grain boundaries. At the same time, the smaller grain boundary area associated with larger grain size is also accounted for and the countering effect of lower grain boundary gas atom saturation inventory at higher exposures is also captured. The net result depends on the power history, i.e., lower fission gas release for low power histories to high exposure and smaller fission gas release during a power excursion. For high power histories, the lower thermal conductivity of Cr-doped fuel enhances gas atom diffusion, such that the effect of larger grain size is practically compensated for.

The Cr-doped fission gas release database is comprehensive, and the full-length fuel rod-average exposure range extends to [ ] as shown in Figure 3-6~~Figure 3-4~~. Based on good data coverage and that no adaptation for Cr-doped fuel was needed for the fission gas release model of RODEX4, that model should be considered valid to a full-length fuel rod exposure of [ ] for Cr-doped fuel as well.

[ ]

3.2.1.2 V&V of the Uniform Corrosion Model for BWR Zircaloy-2 Cladding

The hot-cell examinations that produced the HPU database also include metallographic determinations of the average uniform oxide at the neighboring location to the cut used to determine hydrogen uptake by a high-vacuum fusion and chromatographic measurement of hydrogen. That dataset was used for V&V in Reference 2. More recently, oxide thicknesses have been obtained from fuel rods irradiated in the Plant A2 core for three 24-month cycles, with full-length fuel rod exposures reaching values in the [ ] Results were obtained from fuel rods clad in both RXA and SRA Zry-2 cladding varieties. The RXA fuel rods incorporated Cr-doped fuel while the SRA fuel rods were loaded with non-doped UO_2 pellets. These fuel rods were examined in hot cells. The oxide thicknesses from these fuel rods have been added to the oxide thicknesses shown in Figure 3-8. The oxide layer thickness was at the lower end of the database of the uniform oxide model described above, demonstrating better than expected performance.

3.2.2 G6-Cladding Mechanical Properties

Framatome has a comprehensive database of mechanical tests on irradiated cladding of various metallurgical and zirconium alloy compositions (including data for both SRA and ~~RXS~~ RXA Zircaloy-2 and Zircaloy-4 cladding types). As shown in Figure 3-9, irradiation hardening saturated with fast fluences that correspond to mid-range exposures for existing exposure limits and therefore, extension to higher exposures is appropriate.

The embrittling effect of hydrogen content in combination with irradiation hardening on cladding ductility still satisfies the one percent (1%) uniform strain (elastic + plastic) licensing criterion (see Figure 3-10, for example).

4.0 BEHAVIORAL ASSESSMENT

4.1 *G2 Power Ramp Test and G3 ~~RAI~~ RIA Tests*

[

] The analysis of these AOO transients will continue to be performed based on existing guidance from the NRC that requires compliance with the centerline melting and 1 % criteria. Section 3.3.2 demonstrated that the 1% strain is applicable to the extended exposure range, while the same is true for the melting criterion based on Section 3.1.1.

4.2 *High Burnup Structure*

The high burnup structure (HBS) is a restructuring of the pellet outer rim where the highly increased exposure due to neutron flux self-shielding and Pu buildup leads to matrix recrystallization. This is manifested by appearance of new very small sub-micron grains and very large bubbles (pores) of above one micron in diameter. It has been a concern that HBS might lead to enhanced FGR at high exposure. On the contrary, the research conducted in the last 30 years showed that practically all the gaseous fission products created in the pellet rim are collected in the large HBS pores and hence no additional FGR contribution occurs from the outer pellet HBS zone. This conclusion was reached by comparing the Electron Probe Microanalysis and X-ray Fluorescence studies, the former measuring the gas atom concentration in the matrix (without what is confined in the pores), while the latter captures the total gas concentration that includes matrix and pores.

5.0 UPDATES TO RODEX4 CODE

The RODEX4 encoded methodology was developed as a mechanistic fuel rod analysis code that properly captures the interaction between thermal and mechanical effects for the cladding and fuel. This code includes simplification, when appropriate, using correlations. As a result, the code framework should ensure an accurate prediction of performance at all exposures provided that the models of the different individual phenomena and processes are adequately modeled and validated.

Extended exposure applications of RODEX4 requires a relevant and comprehensive experimental database. Although the mechanistic modeling is a feature of the RODEX4 code, there are several modeling parameters which have been calibrated based on benchmarking specific experimental datasets.

5.1 *RODEX4 Fission Gas Release Model*

As described in Section 3.1.2, the existing fission gas release model remains valid for higher exposures; therefore, no changes are made to the encoded methodology in the RODEX4 code.

5.2 *Cladding Corrosion*

As described in Section 3.2.1, the new cladding corrosion and hydrogen uptake model has been added to the RODEX4 code as an alternative model. The existing oxidation model remains available as an option for use in the downstream safety analyses until ~~they~~ the new model is approved for AFM applications.

5.3 *Extension of NAF RPP Correlations for Higher Enrichments*

The original RODEX4 code radial power profile (RPP) tables had an upper bound of 5 wt% enrichment U-235. For AFM applications fuel enrichment must be increased above 5 wt%, and therefore, the RPP tables have been extended to 10 wt% U-235 enrichment and 10 wt% gadolinia.

The original RODEX4 code included RPP tables derived with [ ] from RPP values generated with [ ] for a range of geometric, operational, fuel composition and enrichment ranges. While the [ ] code was used to generate the power profile values for a range of parameters, the correlation of these values for specific combinations of the relevant parameters was performed with another code, named [ ] This 2000-vintage version of [ ] covered an enrichment range of up to 5 wt% U-235 for commercial PWR and BWR fuel.

Later—after the submittal of RODEX4 topical—an updated versions of [ ] namely [ ] was used to extend the enrichment range to 10 wt% U-235, except for the gadolinia fuel, in which case the maximum U-235 enrichment remained at 5 wt% U-235. These extended RPP tables have been incorporated into the GALILEO fuel code, which was approved recently in Reference 15. The GALILEO RPP tables above the previous limit of 5 wt% U-235 enrichment have been incorporated in RODEX4. Also, the extension of the gadolinia tables above 5 wt% U-235 followed the procedure used for GALILEO.

5.4 *Sample Problem*

To illustrate the performance of Framatome BWR fuel to higher discharge exposures, a sample evaluation was performed with the new version of RODEX4. This sample problem is described and the results obtained are shown in Appendix A.

7.0 UPDATE PROCESS

Framatome plans to continue to acquire fuel rod and fuel assembly performance data on irradiated BWR fuel designs. As poolside post-irradiation examination data for fuel rod bow, fuel rod growth, and fuel assembly growth are obtained, the Framatome PIE databases will be expanded and compared against the licensed bow and growth correlations. If the data support a modification to these correlations, the internal Framatome design change process will be followed. More specifically, modifications or updates to these correlations refer to an update to the fitting parameters or constants of the correlations while the functional forms of the affected correlation(s) will remain unchanged. This change process includes documentation and justification of the change and evaluation of the impact on future design analyses. Any changes to the correlations will be maintained in an internal Framatome document.

For correlation modifications described in Section 6.1.1 Rod bow, the threshold for submittal of an updated correlation for approval by the NRC is an increase or decrease of the correlation upper tolerance limit (UTL) by one standard deviation [ ] relative to the originally approved correlation provided in Reference 3, Appendix A. If PIE data support a correlation UTL reduction of more than one standard deviation, no additional credit may be taken without prior NRC approval.

For Section 6.1.2 Axial Irradiation Growth, the UO_2 differential growth best-estimate and UTL fitting coefficients may be updated with the inclusion of new or revised data such that the revised UO_2 UTL remains within one standard deviation [ ] relative to the submitted correlation (Table 7-1). If PIE data support a correlation UTL reduction of more than one standard deviation, no additional credit may be taken without prior NRC approval.

The chromia-doped enhancement factor and associated correlation coefficients described in Appendix B may be updated [ ] as supported by PIE data collected from chromia-doped fuel rods. The enhancement factor may increase or decrease by [ ] as shown in Table 7-1. If PIE data support a correlation UTL reduction below the stated lower UTL change limit, no additional credit may be taken without prior NRC approval.

The upper and lower change limits to the UO_2 and chromia-doped differential growth correlations are provided in Table 7-1 and shown graphically in Figure 7-1 and Figure 7-2.

A summary of any updates made to these correlations will be communicated to the NRC in the fuel performance interactions which Framatome typically has with the NRC on an annual basis, unless the change exceeds the threshold required for submittal as described above. It is intended that this communication mechanism supersedes the Reference 3 update process mechanism of a letter for information only.

For the RODEX4 fuel rod thermal-mechanical methodology embodied in the initial topical report (BAW-10247-PA, Revision 1), the threshold for updating the methodology remains that of the original SER. Specifically, NRC stated that (SER, Section and L&C 4):

“Due to the empirical nature of the RODEX4 calibration and validation process, the specific values of the equation constants and tuning parameters derived in TR BAW-10247(P), Revision 0, (as updated by RAI responses) become inherently part of the approved models. Thus, these values may not be updated without necessitating further NRC review.”

Table 7-1
UO_2 and Chromia-Doped Differential Growth Upper and Lower UTL Change Limits Allowed without NRC Approval

Figure 7-1
UO_2 Differential Growth UTL Change Limits

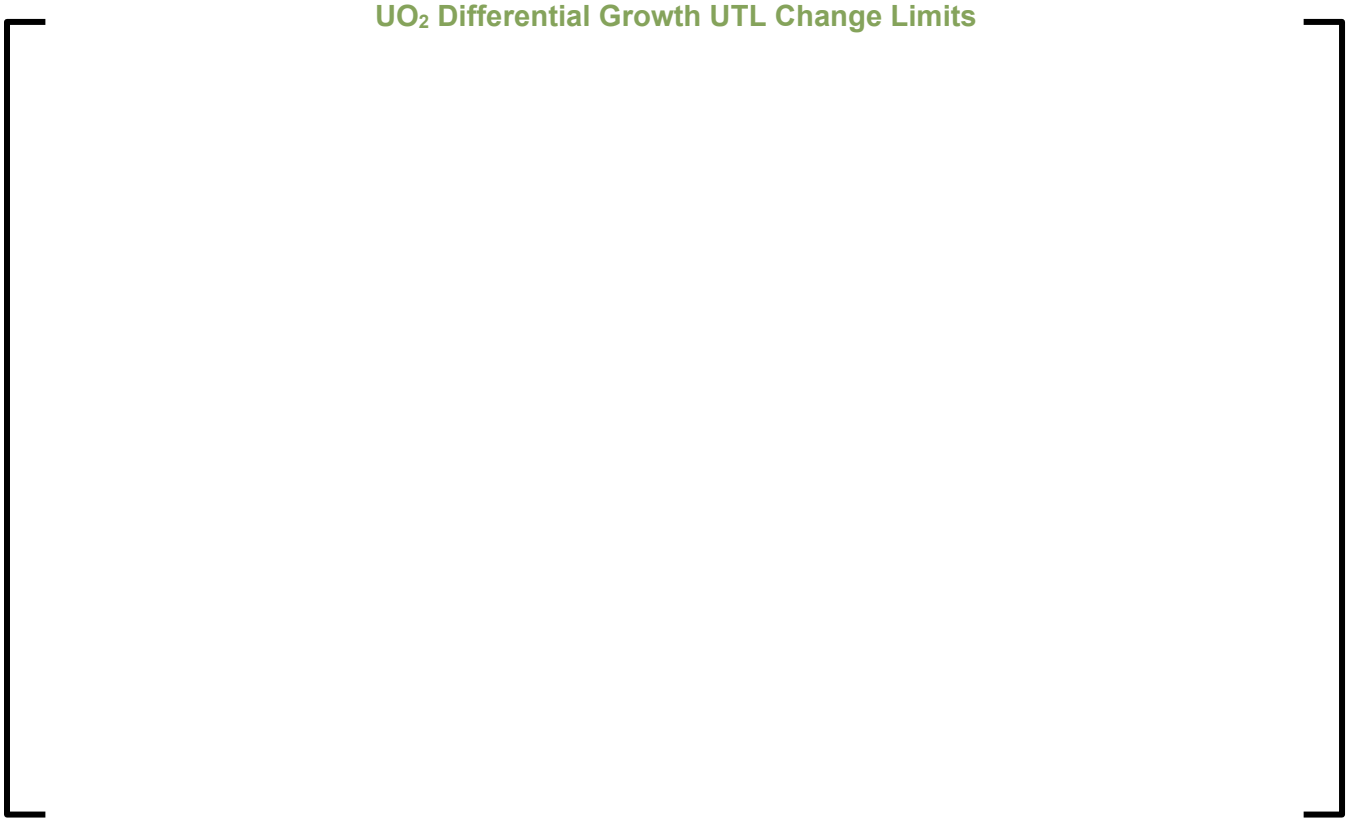

Figure 7-2
Chromia-Doped Differential Growth UTL Change Limits

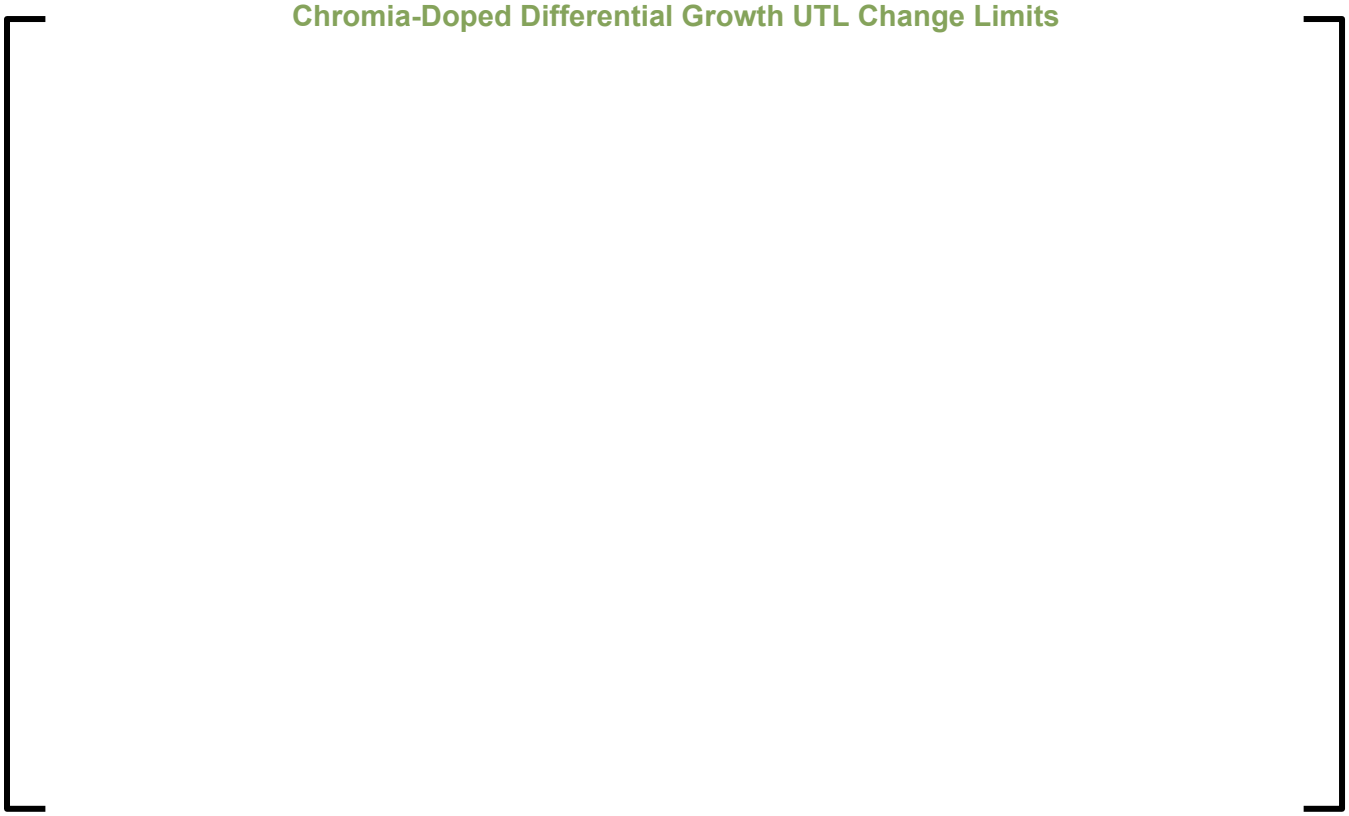

~~Framatome plans to continue to acquire fuel rod and fuel assembly performance data on irradiated BWR fuel designs. As post-irradiation examination data are obtained, the Framatome PIE database will be expanded. Periodically the models in the RODEX4 methodology will be reviewed against the growing database. If the data support a modification to these models, the internal Framatome design change process will be followed. This change process includes documentation and justification of the change and evaluation of the impact on future design analyses. Any changes to the models will be maintained in an internal Framatome document. A summary of any updates made to the models will be communicated to the NRC in the fuel performance interactions which Framatome typically has with the NRC on an annual basis, unless the change exceeds the threshold required for submittal as described below. It is intended that this communication mechanism supersede the Reference 3 update process mechanism of a letter for information only.~~

~~For the methodology changes described in Section 6.0, the threshold for submittal of growth and bow correlations, including the differential growth correlation, is an increase of the correlation tolerance limits by one standard deviation.~~

~~For the RODEX4 methodology, the threshold for submittal depends on the change in the calculated margins for any of the six thermal-mechanical design criteria that are the subject of the methodology. These thresholds are shown in Table 7-1. The difference will be for the same fuel batch analysis and the only change will be the replacement of the model or models. These thresholds represent an increase in the predicted capability of the fuel rod and thus represent a non-conservative change when compared with that reviewed by the NRC in the approval of this methodology.~~

~~If the change is non-conservative, Framatome will either not take credit for the improvement or will submit the change for review and approval before use. If the change represents a conservative change, and reduces the predicted capability of the fuel rod, then no submittal is required.~~

~~Table 7-1~~
~~Thresholds for Design Criteria~~

~~Design Criteria~~	~~Change in Value~~	~~Units~~
~~Clad Tangential Uniform Strain Increment~~	~~0.20~~	~~%~~
~~Pellet Temperatures~~	~~130~~	~~°C~~
~~Fuel Rod Internal Pressure~~	~~1.25~~	~~MPa~~
~~Cladding Fatigue Usage Factor~~	~~0.06~~	~~N/A~~
~~Maximum Clad Oxidation~~	~~8~~	~~µm~~
~~Clad Creep Collapse~~	~~0.125·Cladding Outer Diameter~~	~~mm~~

~~The various models and correlations within the RODEX4 methodology are based on extensive databases covering several fuel designs operating in many different reactors. There is not expected to be a significant change in any of the models or correlations unless a significantly different material is introduced. In such a case, the lead assembly process would be followed prior to reload supply to justify continued use of these models and correlations.~~

10. ANP-10300P-A, Revision ~~1~~0, “AURORA-B: An Evaluation Model for Boiling Water Reactors; Application to Transient and Accident Scenarios,” AREVA NP, ~~December 2009~~January 2018.

11. ANP-10332P-A, Revision 0, “AURORA-B: An Evaluation Model for Boiling Water Reactors; Application to Loss of Coolant Accident Scenarios,” AREVA, ~~February 2014~~March 2019.

12. ANP-10333P-A, Revision 0, “AURORA-B: An Evaluation Model for Boiling Water Reactors; Application to Control Rod Drop Accident (CRDA),” AREVA, March ~~2014~~2018.

13. XN-NF-81-51(P)(A), “LOCA-Seismic Structural Response of an Exxon Nuclear Company BWR Jet Pump Fuel Assembly,’ Exxon Nuclear Company, August 1986.

14. R. Manzel and C.T. Walker, “EPMA and SEM of fuel samples from PWR rods with an average burn-up of around 100 MWd/kgHM,” *Journal of Nuclear Materials* 301 (2002) 170–182.

15. ANP-10323P-A, Revision 1, “GALILEO Fuel Rod Thermal Mechanical Methodology for Pressurized Water Reactors,” Nov. 2020.

16. Letter from J. F. Mallay (AREVA) to Document Control (NRC), "Clarification of Exposure Limit Applicable to Framatome ANP BWR Fuel," NRC:02:029, June 27, 200232-9179540-000.

17. Letter from J. F. Mallay (AREVA) to Document Control (NRC), "Clarification of Exposure Limit Applicable to Framatome ANP BWR Fuel," NRC:02:041, September 4, 2002.

- The maximum cladding oxidation shall be less than [ ] However, this limit was reduced to [ ] when use of the RODEX4 methodology was approved for the used in domestic BWR cores, which is the limit applied in this sample problem.
- The fuel rod internal pressure is limited to be no more than [ ]

To verify that the expected fraction of fuel rods in the batch not exceeding the criteria is at least [ ] the most limiting result of the [ ] cases sampled must be below the limit for each criterion. (Or [ ] cases if the five lowest margin results are discarded, as is the case in this sample problem).

For AOO “slow” transients, in this case flow run-up and CRWE, the specific criteria evaluated, and the numerical limits are:

- The cladding tangential uniform strain, elastic plus inelastic, shall not exceed one percent (1%).
- Pellet temperatures during anticipated transients shall be maintained below melting.
- The fuel rod internal pressure is limited to be no more than [ ]

This third criterion is not strictly applicable to a slow AOO; however, it is necessary for a cycle in which an AOO is experienced (Reference 1, Section 2.2); therefore, margins to this criterion will be reported for this sample problem.

The same number of sample cases as for the steady state operation analysis are performed for each AOO analysis.

APPENDIX B: BWR FUEL ROD TO FUEL ASSEMBLY DIFFERENTIAL GROWTH CORRELATION

Introduction

The data set of ATRIUM™-10, ATRIUM™ 10XM, and ATRIUM™ 11 fuel assemblies that have both fuel assembly and UO_2 SRA fuel rod growth data available is used to develop a differential fuel assembly to fuel rod growth correlation for use in licensing evaluations of fuel rod to upper tie plate clearance. The bases for this correlation development are the observations that:

Measurement Description

Framatome has conducted PIE campaigns both in the U.S. and in Europe to collect fuel rod and fuel assembly growth measurements. The fuel rod growth database includes data from Framatome's legacy designs with 7x7, 8x8, and 9x9 rod arrays which are no longer in operation, and the ATRIUM™-10, ATRIUM™ 10XM and ATRIUM™ 11 designs in use today.

[redacted]

Correlation Development

The method used to develop the differential UO_2 FR/fuel assembly differential growth correlation is fitting the data to a second order polynomial of the form:

$$\boldsymbol{A + B \cdot X + C \cdot X^2 + T} \qquad \text{(B-1)}$$

Table B-1
BWR UO_2 Fuel Rod / Fuel Assembly Growth Correlation

[redacted]

Figure B-2
BWR Fuel Rod Growth Data ~~Correlation~~ for SRA Cladding

Figure B-3
BWR Fuel Assembly Growth Database

Figure B-4
UO_2 Differential Fuel Rod/Fuel Assembly Growth Correlation